Impacts of aerosols and clouds on photolysis frequencies and photochemistry during TRACE-P: 2. Three-dimensional study using a regional chemical transport model

Youhua Tang,[1] Gregory R. Carmichael,[1] Itsushi Uno,[2] Jung-Hun Woo,[1] Gakuji Kurata,[3] Barry Lefer,[4] Richard E. Shetter,[4] Hao Huang,[1] Bruce E. Anderson,[5] Melody A. Avery,[5] Antony D. Clarke,[6] and Donald R. Blake[7]

Received 30 October 2002; revised 17 March 2003; accepted 28 March 2003; published 11 November 2003.

[1] A three-dimensional regional chemical transport model, STEM 2K1, coupled with a detailed radiation model is used to study the influences of aerosols and clouds on photolysis rates and photochemical processes over East Asia-Western Pacific during the TRACE-P period. Measured J-values are compared with those calculated using three-dimensional modeled fields of clouds and aerosols. The model is shown to accurately represent observed J-values over a broad range of conditions. Model studies with and without aerosols and clouds are performed and compared with clear-sky conditions to isolate the various influences. Clouds are shown to have a large impact on photolysis rates during the observation periods of TRACE-P, with J[NO_2] decreased by 20% below clouds and enhanced by ~30% from 1 km to 8 km. Clouds also exert a dominant influence on short-lived radicals, like OH and HO_2. For March, clouds reduce OH by 23% at altitudes below 1 km and increase OH by ~25% above 1 km. Asian aerosols contain large amounts of carbonaceous material, inorganic components such as sulfates, and mineral oxides. These aerosols significantly influence J-values and photochemical processes. When averaged over all TRACE-P DC-8 and P-3 flights, the aerosol influence via affecting J-values reduces OH by ~40% below 1 km, and by ~24% above 1 km. Aerosols have a stronger impact on longer-lived chemical species than clouds do because aerosols tend to be coemitted with precursors and have a longer contact time with the polluted air masses. The accumulated aerosol impact generally is to reduce O_3 concentrations by about 6 ppbv in the biomass burning plumes emitted from Southeast Asia. In megacity plumes, aerosols can increase NO_x concentration by 40% via reducing its photolytic loss and reduce NO_z concentration by a similar amount. A detailed case study of the DC-8 and P-3 flights on 27 March is used to make comparisons for cloud and aerosol influences. During these flights, the cloud impact on J-values is stronger than the aerosol impact, but aerosols are shown to exert a much stronger accumulated influence on O_3 production. *INDEX TERMS:* 0305 Atmospheric Composition and Structure: Aerosols and particles (0345, 4801); 0345 Atmospheric Composition and Structure: Pollution—urban and regional (0305); 0365 Atmospheric Composition and Structure: Troposphere—composition and chemistry; 3337 Meteorology and Atmospheric Dynamics: Numerical modeling and data assimilation; 3359 Meteorology and Atmospheric Dynamics: Radiative processes; *KEYWORDS:* photolysis rates, chemical transport model, TRACE-P, photochemical process, aerosols and clouds, radiative influence

Citation: Tang, Y., et al., Impacts of aerosols and clouds on photolysis frequencies and photochemistry during TRACE-P: 2. Three-dimensional study using a regional chemical transport model, *J. Geophys. Res.*, *108*(D21), 8822, doi:10.1029/2002JD003100, 2003.

[1]Center for Global and Regional Environmental Research, University of Iowa, Iowa City, Iowa, USA.
[2]Research Institute for Applied Mechanics, Kyushu University, Fukuoka, Japan.
[3]Department of Ecological Engineering, Toyohashi University of Technology, Toyohashi, Japan.
[4]National Center for Atmospheric Research, Boulder, Colorado, USA.
[5]NASA Langley Research Center, Hampton, Virginia, USA.
[6]School of Ocean and Earth Science and Technology, University of Hawaii at Manoa, Honolulu, Hawaii, USA.
[7]Department of Chemistry, University of California, Irvine, Irvine, California, USA.

0148-0227/03/2002JD003100$09.00

1. Introduction

[2] Photolysis reactions play a very important role in atmospheric chemistry. Ozone photolysis is the main natural source of the OH radical:

$$O_3 + h\nu(\lambda < 330\ nm) \rightarrow O^1D + O_2$$

$$O^1D + H_2O \rightarrow 2OH$$

The OH radical is the primary oxidizing sink of CO, methane and other hydrocarbons. The chemical generation of ozone in the troposphere also relies on the photolysis reaction of NO_2:

$$NO_2 + h\nu(\lambda < 420\ nm) \rightarrow O^3P + NO$$

$$O^3P + O_2 \rightarrow O_3$$

Considering the importance of photolysis reactions, chemical transport models need to treat photolysis rates (J-values) accurately in order to precisely simulate the photochemical process. However, J-values vary greatly in the atmosphere, and this variability is determined in part by variations in cloud and aerosol optical depths. *Martin et al.* [2000] showed the importance of cloud estimates to UV irradiance. *Dickerson et al.* [1997] revealed the impacts of different aerosols on photochemical smog, based on their optical properties. *He and Carmichael* [2001] employed a one-dimensional radiation model to study the sensitivity of photolysis rates and ozone production. *Martin et al.* [2003] used a global model to make sensitivity study, and indicated that surface J[O^1D] decreased 5–20% in the Northern Hemisphere, mainly due to mineral dust, and biomass burning plumes had the strongest influence.

[3] The Transport and Chemical Evolution over the Pacific (TRACE-P) experiment provides an excellent opportunity to test our capabilities to model photolysis rates and to study the effects of clouds and aerosols. This experiment was performed with two NASA aircrafts (DC-8 and P-3) over western Pacific-East Asia from the end of February to early April 2001 [*Jacob et al.*, 2003]. The DC-8 flights had an altitude variation from 150 m to 12 km, and the P-3 flight altitudes ranged from 150 m to 7 km. More than 100 chemical species, at least 20 aerosol-related variables [*Jacob et al.*, 2003; *Weber et al.*, 2003; *Jordan et al.*, 2003] and meteorological information were measured in both of the aircrafts. During TRACE-P period, photolysis frequencies were determined by actinic flux spectroradiometry technique [*Shetter et al.*, 2002] and reported by *Lefer et al.* [2003]. Simultaneous measurements of many photochemistry-related species and aerosol quantities were also obtained. This joint dataset provides detailed information about photolysis rates and associated variables in this region.

[4] During the springtime in the Asia-Pacific region, continental outflow is heavily influenced by aerosols. Biomass burning plumes contain large quantities of carbonaceous aerosol, volcanic plumes contain sulfate particles, Asian megacities contain large amounts of primary and secondary anthropogenic aerosol, and dust storms provide an abundant source of mineral aerosols. Furthermore, during the springtime the southeast monsoon brings warm and humid air to this region and causes significant cloud formation. Thus these East Asia outflow events provided an excellent location to test our ability to model photolysis rates.

[5] Here we evaluate the online calculation of photolysis rates in our three-dimensional chemical transport model. In addition we study the effects of aerosols and clouds on the photochemical processes. *Lefer et al.* [2003] presented their analysis of the observed data for the TRACE-P experiment.

2. Model Description

[6] In this study we employ a three-dimensional regional chemical transport model, STEM 2K1, developed by University of Iowa, as the basic research model. The STEM version 2K1 employs the standard z-coordinate for the transport computation:

$$\frac{dC}{dt} = u\frac{\partial C}{\partial x} + v\frac{\partial C}{\partial y} + w\frac{\partial C}{\partial z} + D_v + D_h + E + L_{chem}$$

where C is the species concentration and D_v and D_h are the contributions from vertical and horizontal diffusions, respectively. E is the emission term, and L_{chem} is the concentration changes due to chemical reactions. The vertical coordinate z is represented as the absolute height above sea level. STEM 2K1 does not require a uniform horizontal grid system.

[7] The Galerkin scheme [*McRae et al.*, 1982] is the default scheme for advection computations in STEM 2K1. The advection computations are split in three directions and performed in the following sequence:

$$\begin{aligned}\mathrm{Advec.(X)} \rightarrow \mathrm{Advec.(Y)} \rightarrow \mathrm{Advec.(Z)} \rightarrow \mathrm{Advec.(Z)} \\ \rightarrow \mathrm{Advec.(Y)} \rightarrow \mathrm{Advec.(X)}\end{aligned}$$

Since we can treat the advection computation separately for each direction, source code parallelization becomes relatively easy [*Miehe et al.*, 2002]. The computing speed enhancement due to parallelization is important because it enables the model with complex chemical mechanism and high resolution to be used in real-time forecast applications. During the TRACE-P and ACE-ASIA field campaigns, the parallelizated STEM 2K1 successfully provided not only an 80 km-resolution forecast but also a 16 km-resolution nested real-time prediction with the SAPRC99 mechanism [*Carter*, 2000]. These forecasts were used in flight planning activities. *Miehe et al.* [2002] provided a detailed description of the STEM 2K1 parallelization and performance. Calculations of this model were run on a Linux cluster.

[8] The STEM model as used in this experiment and its comparison with observed TRACE-P data is presented in the work of *Carmichael et al.* [2003]. In this study photolysis rates were calculated on-line within STEM using the NCAR Tropospheric Ultraviolet-Visible (TUV) radiation model [*Madronich and Flocke*, 1999]. As a one-dimensional column model, TUV considers the influences of clouds, aerosols, and gas-phase absorptions due to O_3, SO_2, and NO_2. In our simulations, all of these variables were calculated by the STEM. Cloud fields were originally calculated by the RAMS mesoscale meteorological model. For TRACE-P simulation,

the simplified Kuo cumulus parameterization [*Tremback*, 1990] was used to represent the subgrid scale cumulus convection along with Kessler-type microphysics [*Walko et al.*, 1995]. The microphysics module in RAMS is capable of simulating mesoscale clouds and precipitation phenomena. For photolysis calculations, we kept track of water clouds and ice clouds. STEM employs RAMS outputted cloud water content to derive cloud optical properties. The optical properties of water clouds were calculated with a simple scheme [*Madronich*, 1987]. We adopted the method of *Ebert and Curry* [1992] to estimate ice cloud optical properties. Aerosols fields were calculated within the STEM model. We modeled explicitly black carbon (BC), organic carbon (OC), sulfate, sea salt, wind blown dust, and primary mineral aerosols from cities (e.g., from roads and construction). The BC simulation is mentioned by *Carmichael et al.* [2003], and we will discuss our dust simulations in the work of *Tang et al.* [2003a, 2003b]. At each integrating time step, the online TUV inputs these aerosol concentrations from the STEM main module and converts them from mass concentrations to aerosol optical properties according to *Hess et al.* [1998]. Here we assume all aerosols are mixed externally. In this study, we employed a domain with 80 km horizontal resolution that covered most of East and Southeast Asia. The RAMS model was driven by ECMWF $1^\circ \times 1^\circ$ reanalysis data. The modeled meteorological data was also used to derive dust, lighting NO_x, sea salt, and biogenic emissions.

[9] A schematic of the interactions of TUV with STEM is shown in Figure 1. In these simulations, TUV was called every 10 min, and just before STEM performed the chemical calculations. The online TUV was two-way coupled with STEM's other modules: input concentrations of aerosols and gas-phase species (O_3, NO_2, SO_2), and output 30 photolysis rates for SAPRC99 mechanism. Here the TUV has a higher top (80 km) than that of the chemical-transport domain ($\sim$15 km). The upper layers were used to compute the ozone absorption. To consider this impact, ozone column concentrations are necessary. In our simulations, daily variations in ozone columns were accounted for by using the observed TOMS (Total Ozone Mapping Spectrometer) total columns. Zonal mean values were used for the regions that the TOMS satellite did not cover. Then the pasted TOMS data was interpolated to the STEM domain. Ozone profiles calculated by STEM were used in TUV for the tropospheric component, and the upper atmosphere ozone absorption column was calculated by the difference between TOMS ozone and STEM column ozone. We assumed that this upper atmosphere ozone had a vertical distribution as defined by the US standard atmosphere-1976.

[10] Here we employed the SAPRC99 gas-phase chemical mechanism [*Carter*, 2000] and the second-order implicit Rosenbrock method [*Verwer et al.*, 1999] for the chemical integrator. We utilized the kinetic preprocessor [*Damian et al.*, 2002] to interface the chemical processes with STEM. SAPRC99 contains 213 chemical reactions, including 30 photolysis reactions. Dry deposition velocities were calculated based on the parameterization of *Wesely* [1989].

3. Emissions

[11] The STEM model utilized energy and field combustion emissions developed especially for this study. The energy-related inventory used is described by *Streets et al.* [2003] and the biomass burning emissions are presented in the work of *Woo et al.* [2003]. The biogenic emissions were driven by the mesoscale meteorological prediction and utilized a biogenic emissions model based on the work of *Guenther et al.* [1995] and modified for China as provided by Allison Steiner (Georgia Institute of Technology).

[12] Volcanic emissions contributed a significant amount of SO_2. The Geological Survey of Japan reported that Mt. Miyakajima emitted SO_2 up to 40,000 Ton/day during the TRACE-P period. This can be compared with the total anthropogenic SO_2 emission in China, which are estimated to be $\sim$56,000 Ton/day. Aviation emissions were taken from EDGAR [*Olivier et al.*, 1996]. Lightning NO_x emissions were diagnosed from the meteorological model according to deep convective intensities [*Pickering et al.*, 1998].

[13] Emissions of wind blown soil, generated from the arid and semi-arid regions in Asia, were calculated on-line using model calculated friction velocities according to the method of *Nickling and Gillies* [1993] and *Liu and Westphal* [2001]. Sea salt emissions were also calculated on-line following *Monahan et al.* [1986].

4. Results and Discussion

[14] To study the influences of clouds and aerosols on photolysis rates three simulations were performed: STEM with online TUV under normal conditions (NORMAL), under clear sky condition (CLEARSKY), and without considering aerosol impacts on radiation (NOAOD). The normal simulation refers to the case where we explicitly consider the cloud and aerosol impacts on radiation transfer. The CLEARSKY simulation does not consider either of these impacts and the NOAOD considers only the cloud influence. All of these simulations consider the absorption of gas-phase species. Except for the photolysis calculations, all other settings are the same for these simulations.

4.1. Overview of J-Value Simulations and Influencing Factors

[15] Figure 2 shows the comparison between the simulated and observed J-values for the TRACE-P DC-8 and P-3 flights from 3 March to 2 April 2001. The observed values every five minutes along the flight tracks are plotted against the calculated values sampled from the three-dimensional model results for the same times and locations (using trilinear interpolation in space). As a complex experiment, TRACE-P deployed many different measuring instruments, and each instrument has its own sampling frequency. *Lefer et al.* [2003] described the measurements of photolysis rates boarding on the two aircrafts. To compare these data with modeled results, we used all data in 5-min intervals. Throughout this paper, all plots showing data symbols refer to the points every 5 min along the flight paths. The model has significant skill in calculating J-values. Figure 2 shows that simulated J-values are highly correlated with the observed ones, with the correlation coefficients R varying from 0.80 to 0.95 for the four photolysis rates. The simulations agree better with the observations in the mid-range of J-values than in very low or very high J-value ranges.

[16] Clouds play a critical role in affecting the photolysis rates. We compared several flight periods with few broken

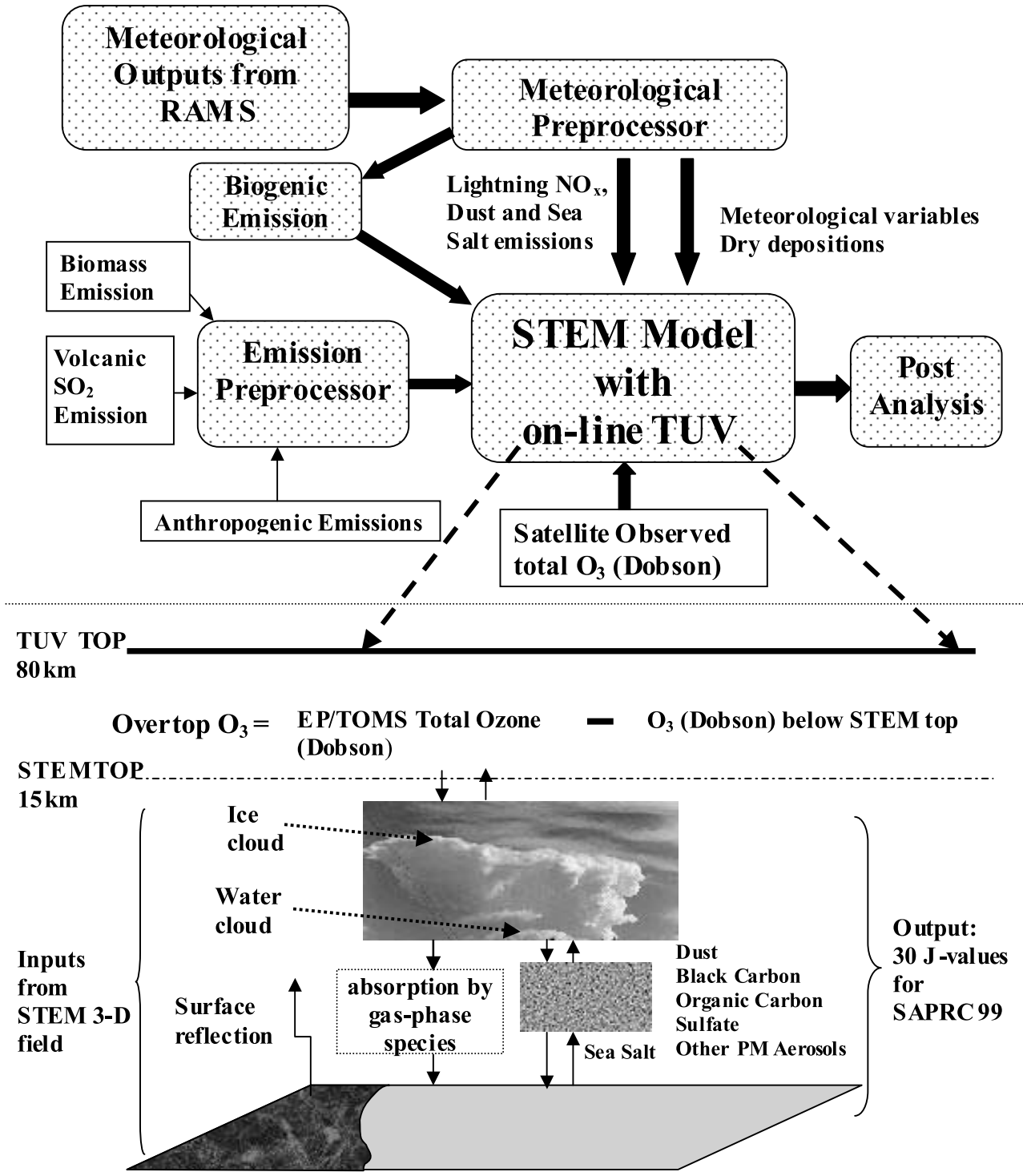

Figure 1. Framework of STEM and its online TUV data flow.

clouds and low aerosol loading to the CLEARSKY simulation, and the correlation coefficients for J-values (those R are 0.98, 0.88, 0.98, and 0.99 for $J[O^1D]$, $J[NO_2]$, $J[CH_3CHO]$ and J[Acetone], respectively) for this subset of the data were significantly higher than for the cloud and aerosol conditions. This shows the online TUV model performed well. However, clouds are a major source of uncertainty in calculation. Among these four photolysis rates, $J[NO_2]$ has the strongest sensitivity to clouds and shows the largest spread between predicted and observed. We attribute the underestimation of $J[NO_2]$ at low values and overestimation at high values to features in the predicted cloud fields. While the RAMS model generally provided reasonable cloud information for most flights, it is very difficult to produce quantitative information on clouds with the relatively coarse resolution (80 km horizontal resolution) used in these calculations.

[17] Another important influencing factor is aerosols. During TRACE-P a variety of aerosol optical properties

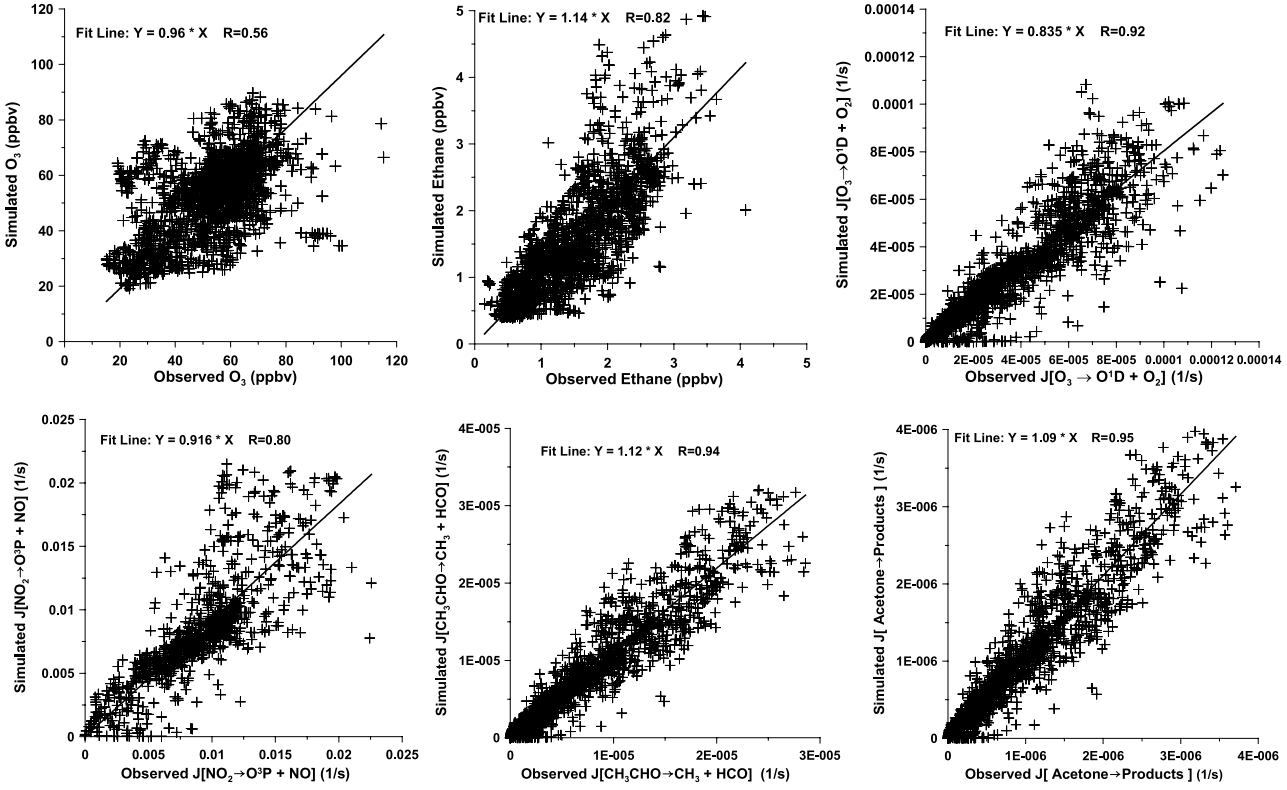

Figure 2. The correlations of O_3, Ethane and 4 J-values between STEM NORMAL simulation and observations for All TRACE-P DC-8 and P3 flights.

were measured, including aerosol absorption and scattering coefficients. *Jacob et al.* [2003] listed the measurements taken on these two aircrafts. The model predicted aerosol optical extinction coefficient (AOE) at wavelength of 550 nm is consistent with the observations as shown in Figure 3. The simulated AOE agrees well with the observation in most events, though missing some very high values at low altitudes. AOE has a very significant gradient in the vertical, with most aerosols concentrated in the boundary layer. These high observed values of AOE tended to be associated with encounters with volcanic plumes, dust events, megacity plumes, and biomass burning events. However. it is important to note that there does not appear to be a strong bias in either the cloud or aerosol distributions.

[18] Further insights into the observed and modeled J-values are found in Figure 4, where J-values are plotted as a function of local time. Three calculated cases are presented: the NORMAL, CLEARSKY, and NOAOD. The NORMAL simulation is shown to accurately represent the diurnal variation. Owing to the model's coarse resolution and uncertainties in the meteorological prediction, some underestimations or overestimations exist for the prediction for the cloud position and optical depth, especially for fractional clouds. For example, the model sometimes overpredicted clouds, and some realistic fractional clouds were treated as overcast clouds and yield very low J-values.

[19] As expected, the CLEARSKY simulation has a significant systematical bias from the observed values, especially for $J[NO_2]$. The CLEARSKY simulation overestimates photolysis rates under clouds and underestimates above clouds. These results clearly show the two major impacts that clouds play on photolysis rates: the shielding effect under clouds and the reflecting effect above clouds. The effects of aerosols can be seen in the NOAOD simulations. When aerosols are removed but clouds remain, we see that the calculated $J[NO_2]$ and $J[O^1D]$ values increase significantly near local noon time. The TRACE-P measurements clearly show a large influence of clouds and aerosols.

[20] The effects of clouds and aerosols on the vertical distribution of photolysis rates are presented in Figure 5. Correspondingly, Table 1 shows the averaged effects in three layers. Shown in Figures 5a and 5b are the differences between the NORMAL and NOAOD runs, which gives the influence of aerosols in the presence of clouds, and the difference between the NOAOD and CLEARSKY simulations, which gives the effects of clouds. In the presence of clouds, photolysis rates are decreased significantly below ~1.5 km and enhanced throughout the troposphere. Our simulations show that on average over all the TRACE-P flights during this period, clouds decrease $J[NO_2]$ and $J[O^1D]$ by 22% below 1 km. In the upper layers (above 3 km), both $J[NO_2]$ and $J[O^1D]$ show significant enhancements due to cloud reflection. On average, $J[NO_2]$ was enhanced by 34%, and $J[O^1D]$ was enhanced by 23% due to clouds for flights above 3 km. Generally, $J[NO_2]$ is more sensitive to cloud reflection than $J[O^1D]$ and most other J-values. Depending on cloud height and thickness, these enhancements of J-values due to cloud reflection can extend throughout the troposphere. The flight logs of these two aircrafts reported visible cloud information. Especially the P-3 aircraft, which flew at relatively low altitude, had detailed cloud description. Except for the scenarios of big

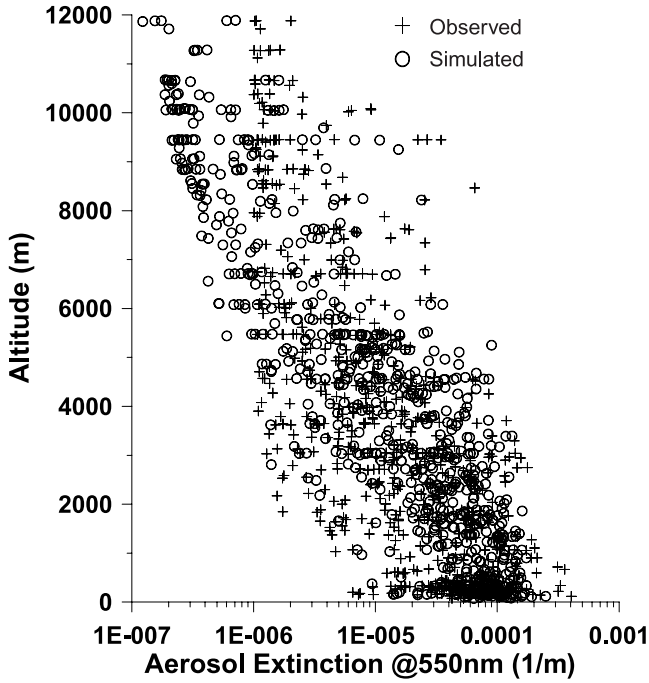

Figure 3. Observed and simulated aerosol extinction coefficients distributed in altitude for all TRACE-P flights.

events, like frontal outflow, most clouds encountered by the aircrafts were oceanic boundary layer cloud, with the altitudes from 300 m to 2 km. Both aircrafts reported numerous encounters with haze layers, which reflect the high aerosol loading at high humidity in this region.

[21] Asian outflow contains large amounts of all kinds of aerosols and usually contains a significant amount of BC, which is highly absorptive. The aerosol properties of the outflow airmass are similar to the mixing aerosols described by *Liao et al.* [1999]. The averaged aerosol single scattering albedo for all TRACE-P flights was 0.823, reported by the measurements. The aerosol may become more absorptive in biomass burning plumes [*Tang et al.* 2003a, 2003b]. The presence of these absorptive aerosols tends to decrease J-values in all altitudes. On average, our simulations show that aerosols decreased $J[O^1D]$ by about 38% and $J[NO_2]$ by 35% for all TRACE-P flights below 1 km and decreased $J[O^1D]$ and $J[NO_2]$ by 20% for the flights above 1 km.

4.2. Influences of Clouds and Aerosols on Chemical Species

[22] The three simulations discussed above show that aerosols and clouds have significant impacts on J-values. Certainly, these impacts also influence the distributions of photochemical species. Figure 5 shows profiles of the influences of aerosols and clouds on several species along with the DC-8 and P-3 flight paths. The impacts of clouds and aerosols on OH and HO_2 via changing J-values are

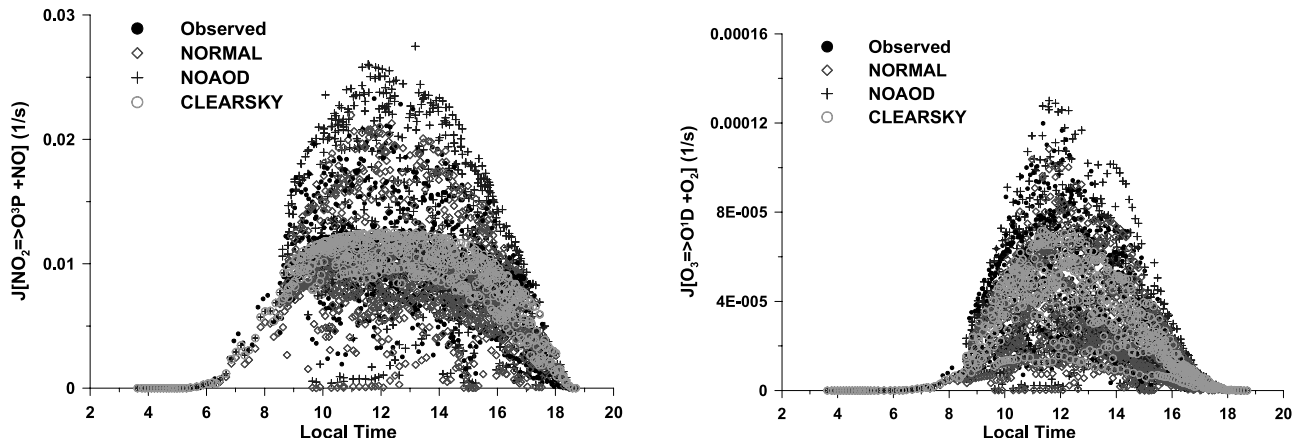

Figure 4. Observed and simulated $J[NO_2]$, $J[O^1D]$ for All TRACE-P DC-8 and P-3 flights under three conditions: NORMAL, NOAOD, and CLEARSKY, distributed in local time. See color version of this figure at back of this issue.

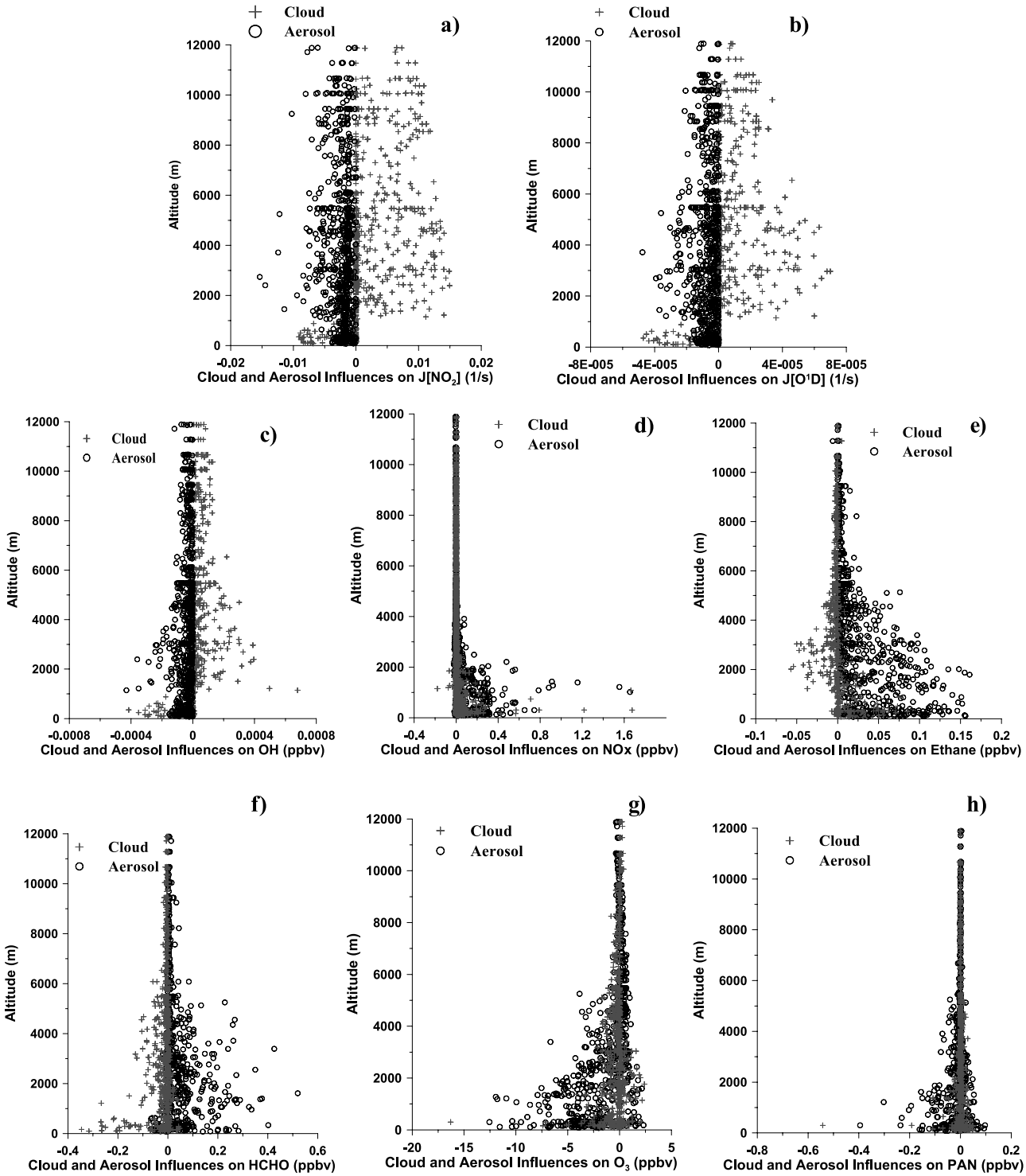

Figure 5. Observed and simulated aerosol and cloud influences on J[NO_2], J[O^1D], OH, NO_x, Ethane, HCHO, O_3, and PAN for all TRACE-P DC-8 and P3 flights in vertical profiles. The aerosol influences are represented in NORMAL minus NOAOD simulations, and clouds influences are represented in NOAOD minus CLEARSKY. See color version of this figure at back of this issue.

Table 1. Averaged Aerosol and Cloud Influences Along the Paths of All TRACE-P DC-8 and P-3 Scientific Flights Merged in Three Vertical Layers, Represented in Percentage Change (Some Significant Influences are Highlighted With Bold Font)

Species and Variables	Cloud Influences			Aerosol Influences		
	<1 km	>1 km but <3 km	>3 km	<1 km	>1 km but <3 km	>3 km
O_3	−1.2%	−0.38%	−0.36%	**−4.8%**	**−3.2%**	−0.06%
Ethane	0.75%	−0.28%	−0.30%	3.1%	2.8%	1.1%
Formaldehyde	**−6.1%**	−3.2%	−4.2%	4.8%	**13.2%**	**6.7%**
OH	**−23.4%**	**21.7%**	**27.7%**	**−39.8%**	**−31.4%**	**−19.2%**
NO_x	**16.1%**	8.9%	8.71%	**16.6%**	**15.0%**	−0.81%
PAN	2.1%	0.63%	0.20%	**4.4%**	1.4%	0.46%
$J[NO_2]$	**−21.6%**	**22.5%**	**34.1%**	**−35.5%**	**−27.2%**	**−17.7%**
$J[O_3 \rightarrow O_2 + O^1D]$	**−21.8%**	**16.7%**	**22.8%**	**−38.5%**	**−29.2%**	**−17.4%**

quite similar to their influence on J-values because these radicals are sensitive to local J-values and are governed by fast chemical processes. *Lefer et al.* [2003] used a photochemical box model and in situ measured data to check the sensitivity of OH to the local J-value variation and found that the OH variation was nearly linearly correlated with the J-value variation. In our study, compared with its influences on J-values, cloud effects on OH are amplified because a main source of OH (the reaction $O^1D + H_2O \rightarrow 2OH$) is positively correlated with water vapor concentration. If we exclude temperature perturbation, the water vapor concentration could be represented by relative humidity, which is high in and near clouds. Since HO_2 concentrations are highly correlated with OH through a series of fast reactions, the response of HO_2 is similar to that for OH. On average the aerosol influence is shown to decrease OH levels by 40% below 1 km and ~24% at higher altitudes. Clouds reduce OH by ~23% at altitudes below 1 km, but increase OH by ~25% above.

[23] The impact of perturbations of photolysis rates on longer-lived species is more complicated. For example, as shown in Figure 5d, the presence of clouds and aerosol increases NO_x levels in the boundary layer, due to the decrease in the photolytic loss of NO_2 and to a decrease in OH and HO_2 levels. Similar impacts are also seen for primary reactive hydrocarbons, such as ethane (Figure 5e), which can be simply explained by the corresponding impacts on OH. The reaction between ethane and OH can be a source of acetaldehyde and formaldehyde:

$$C_2H_6 + OH + O_2 \rightarrow C_2H_5O_2 + H_2O$$

$$C_2H_5O_2 + NO \rightarrow C_2H_5O + NO_2$$

$$C_2H_5O + O_2 \rightarrow CH_3CHO + HO_2$$

$$CH_3CHO + OH \rightarrow CH_3CO + H_2O$$

$$CH_3CO + HO_2 \rightarrow HCOOH + HCHO$$

The impact on secondary photochemical active species is even more complicated. For example, both the formation and destruction of formaldehyde can be initiated by reactions involving OH, and it also can be photodissociated directly. Model results shown in Figure 5f suggest that the net effect of aerosols in general is to increase HCHO levels throughout the troposphere by up to 0.5 ppbv. The cloud impact on HCHO depends on altitude. The decrease of HCHO in higher layers is due to the decrease of hydrocarbon concentrations and higher HCHO photolysis rates. In the lower layers, the existence of clouds leads to a decrease in photolysis rates and an increase in most primary hydrocarbon concentrations. In principle, the HCHO concentration might be expected to increase. However, the low OH concentration can slow down the HCHO production rates. Thus the net cloud influence on HCHO in the low altitudes varies from case to case, depending on the characteristics of the airmass.

[24] Although PAN is also a photochemical product generated from emitted pollutants NO_x and NMHCs, the aerosol and cloud influences on PAN differ significantly from those influences on HCHO. As a relatively long-lived species, the PAN levels depend not only on local NO_x concentrations but also on transport. Since its lifetime is longer than NO_x, PAN concentrations are more strongly affected by transport than by local production on most of the TRACE-P flights. So while aerosols and clouds increase local NO_x, the PAN concentrations do not show a corresponding enhancement, but usually show a decrease in polluted airmass. Since photochemical reactions are slowed down due to aerosols, the PAN production rates decrease in the NO_x source regions, and as a result PAN concentrations are reduced. The reduction of PAN due to aerosol influence can be up to 0.4 ppbv in the TRACE-P flight paths. However, in low NO_x conditions, the aerosol impact on PAN is mainly to increase its concentration by decreasing its photolysis rate, which explains the positive averaged influence on PAN (Table 1). The cloud impact on PAN is similar to the aerosol impact in the lower layers but weaker. The cloud and aerosol influences on O_3 are quite similar to those influences on PAN. Generally, in pollutant plumes, decreases in J-values cause lower O_3 concentrations due to lower photochemical production. This O_3 reduction due to aerosols could be up to 12 ppbv. In low NO_x conditions aerosols usually increase O_3 by decreasing its photolysis loss, and clouds tend to decrease above-cloud O_3 by enhancing photochemical loss.

[25] When averaged over TRACE-P flights, aerosol influences on most species via affecting photolysis rates are higher than the corresponding cloud influences in the lower layers (Table 1). However, as shown by Figure 5g, the biggest influence (16 ppbv O_3 decrease) comes from clouds, though these scenarios are not frequent. Since the cloud optical depths are usually much higher than aerosol optical

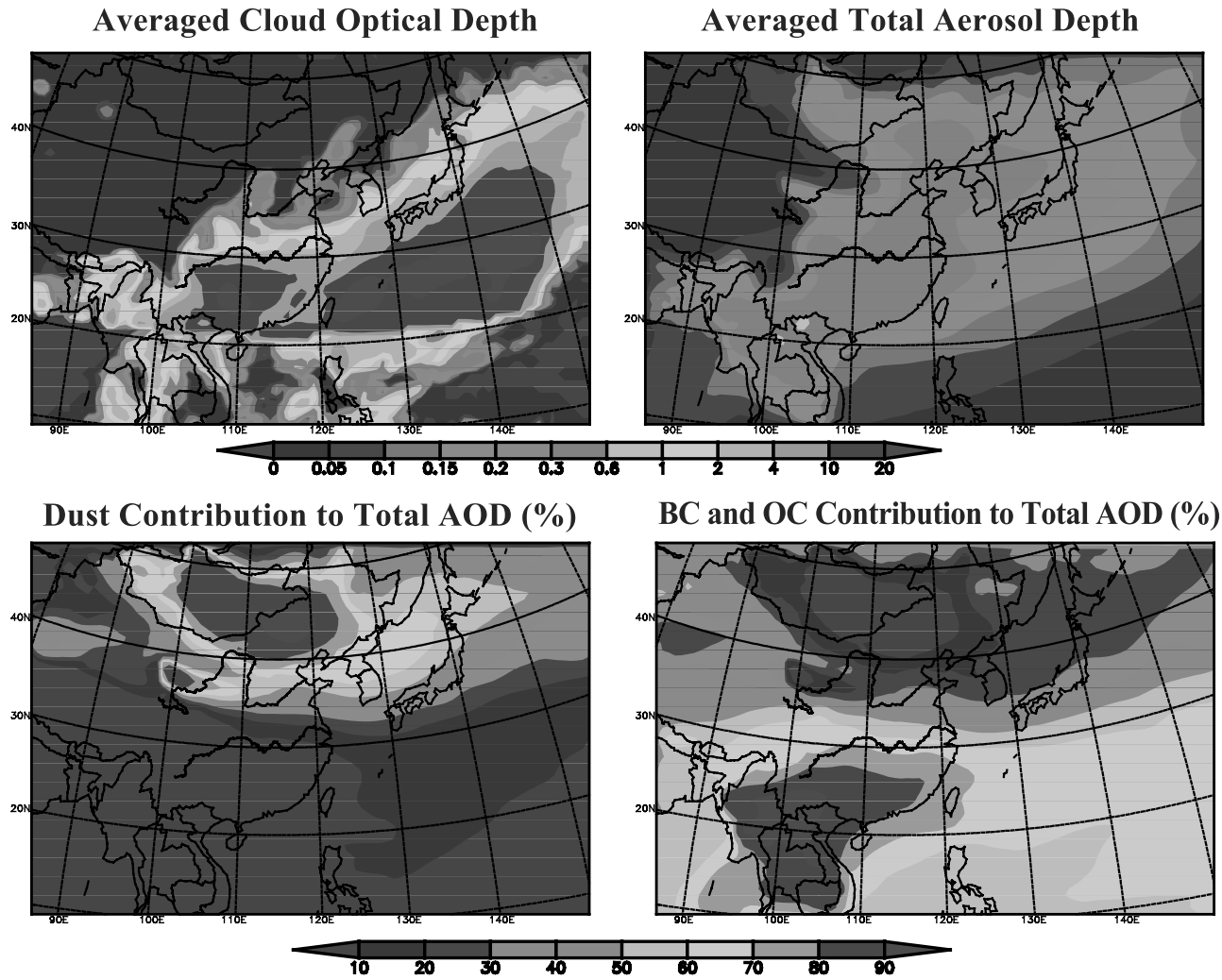

Figure 6. March-averaged simulated cloud optical depth, aerosols optical depth, and the fractional contributions from dust, BC, and OC. See color version of this figure at back of this issue.

depths, clouds can exert significant influences on chemical species. The reason why aerosols tend to have a stronger influence than clouds is due to the fact that aerosols are usually transported along with the pollutants in megacity, biomass burning, and biofuel plumes. These aerosols can stay correlated with the photochemical oxidants and precursors over synoptic time scales (several days).

4.3. Three-Dimensional Structure of Cloud and Aerosol Influences on Chemical Species

[26] The results presented so far are those along the flight paths. During TRACE-P the DC-8 and P-3 flew almost exclusively over the sea. Using the model results we can evaluate the horizontal variations in the aerosol and cloud effects over all of East Asia, and identify where the effects are expected to be largest. For reference, the average cloud and aerosol optical depths are presented in Figure 6. As discussed previously, the averaged cloud optical depths are $\sim$50 times larger than the aerosol values, but individual clouds are short-lived. Another important point is the spatial locations of the optical depths. The cloud optical depths highlight the average frontal position during this period, while the aerosol distributions are displaced due to the spatial locations of the major emission sources: the biomass burning (BB) region, dust region, and the high fuel-related emission regions in East Asia. The BB aerosols (mainly BC and OC) dominate the aerosol optical depths (AOD) in the south region (include Southeast Asia and South China), and the dust contribution is the major part of AOD in Mongolia and North China. Although the dust AOD and BB AOD are similar in magnitude, their appearances and influences are quite different. Dusts, like clouds, occur occasionally, and the dust regions do not have strong pollutant emissions. Biomass burning emissions occur frequently during this period in Southeast Asia, and BB plumes contain large amounts of pollutants that accompany aerosols in the outflow.

[27] Figure 7 shows the March-averaged horizontal distribution of the effects of clouds and aerosols on daytime $J[O^1D]$ rates for the low, middle, and upper regions of the troposphere. Biomass burning aerosols tend to show a closer spatial correlation with clouds due to the fact that BB emissions come largely from South East Asia during this period and are transported in the warm sector of cold fronts. Anthropogenic emissions are highest north of 25°N, and are transported off the continent mostly in the region

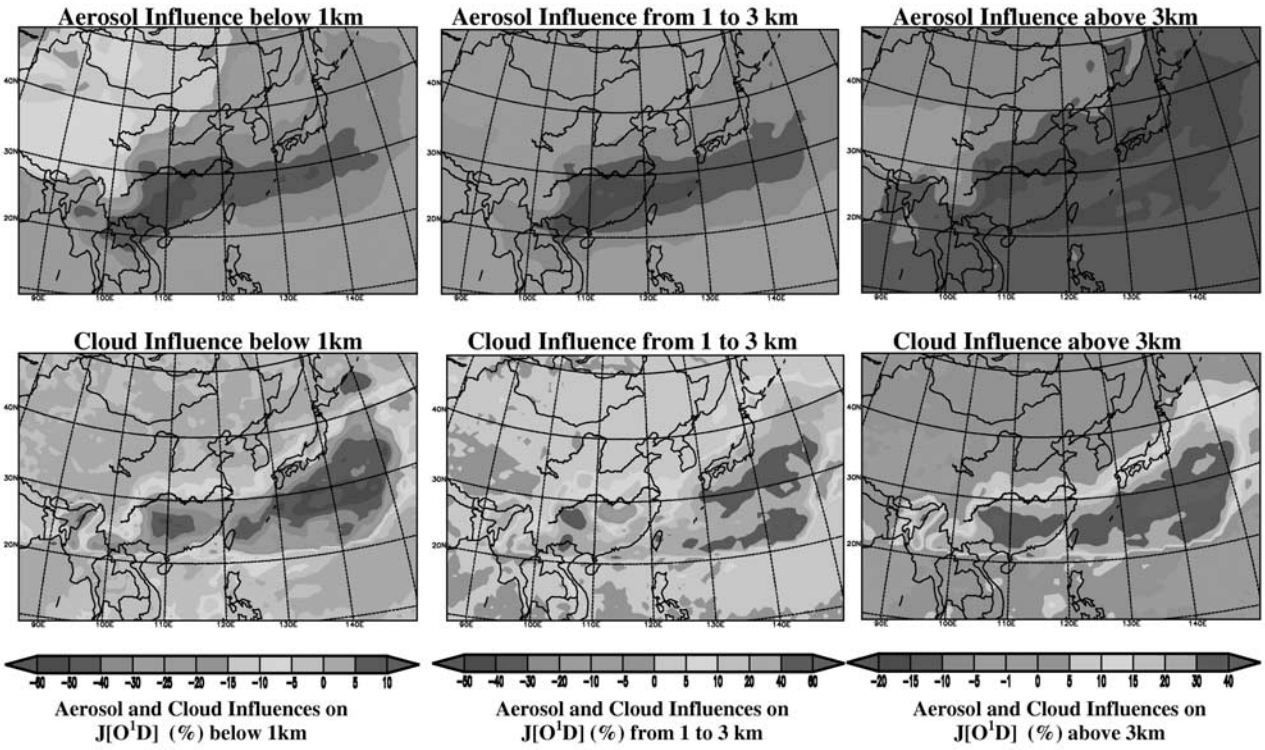

Figure 7. March-averaged aerosol and cloud influences on daytime $J[O^1D]$ in three layers: below 1 km, 1 to 3 km, and above 3 km, represented in percentage change. See color version of this figure at back of this issue.

between 30° and 40°N. The importance of clouds on photolysis rates is clearly seen. On average above 1 km, the presence of clouds enhances $J[O^1D]$ by up to 60% (or 1.4×10^{-5} s^{-1} in absolute change) and covers almost the entire latitudinal band from 20° to 25°N. Near the surface clouds reduce photolysis rates as discussed previously.

[28] The aerosol influence is smaller and opposite that for clouds in layers above 1 km. In the lowest 1 km, the main decrease of $J[O^1D]$ (up to 60%, or 1.2×10^{-5} s^{-1} in daytime average) is due to aerosols over the biomass burning source regions in Southeastern Asia. Above 1 km the areas with strong aerosol effects lie west of 110°E and east of 135°E. This is the outflow location of the biomass burning plumes, and it is located a bit north of the location of maximum cloud cover illustrating that pollutants and water are transported within these fronts of different locations.

[29] The effects of clouds and aerosols on OH levels are shown in Figure 8. In general, the cloud and aerosol influences on OH are similar to their influence on $J[O^1D]$ for all layers. On average clouds and aerosols reduce OH by up to 60% below 1 km. In the layers above 1 km, aerosols reduce OH up to 40% in biomass burning regions and clouds enhance OH by 50% in the western Pacific. The cloud influence on OH is stronger than that on $J[O^1D]$ above 3 km because the rich water vapor in cloudy regions can exacerbate this influence. The aerosol influence on OH are stronger than those on $J[O^1D]$ below 3 km. The strong OH reducing areas (50% for the layer below 1 km, 40% for the 1–3 km layer) are larger than the corresponding $J[O^1D]$ reducing areas. OH is affected not only by local J-values but also by ambient CO, VOCs, and NO_x levels. Since the transported pollutants are increased due to the reduced OH concentration, the feedback effect causes a decrease of OH in the downwind areas. In this manner the aerosol influence on OH is extended all along the pollutant transport path. The cloud and aerosol influences on HO_2 are similar to their influences on OH.

[30] In the case of ozone, clouds are shown on average to decrease ozone levels in and below the cloudy regions (Figure 9). The presence of aerosols also reduces ozone levels in the outflow regions, but the effects are spatially distributed in a much different manner than those due to clouds. The largest effects of aerosols are found in the major ozone production regions, such as the biomass burning regions in Southeast Asia and over the major urban centers such as Shanghai and Tokyo. Over Shanghai aerosols reduce daytime O_3 by an average of 15%. In the 1 km to 3 km layer, ozone within the biomass burning plumes reduced by up to 5 ppbv (8%). On the southern edge of the modeling domain, ozone levels are enhanced due to aerosols. This is related to the fact that NO_x lifetimes are increased and more NO_x is transported to these NO_x limited regions, resulting in some enhanced ozone production.

[31] As discussed above, reducing O_3 photochemical production is the main effect of both clouds and aerosols on O_3 in polluted airmass. Our simulations show that CO is also affected by the aerosol reducing J-values and that CO increase by about 6 ppbv in the region covered by biomass burning plumes. The biggest relative influences occur for

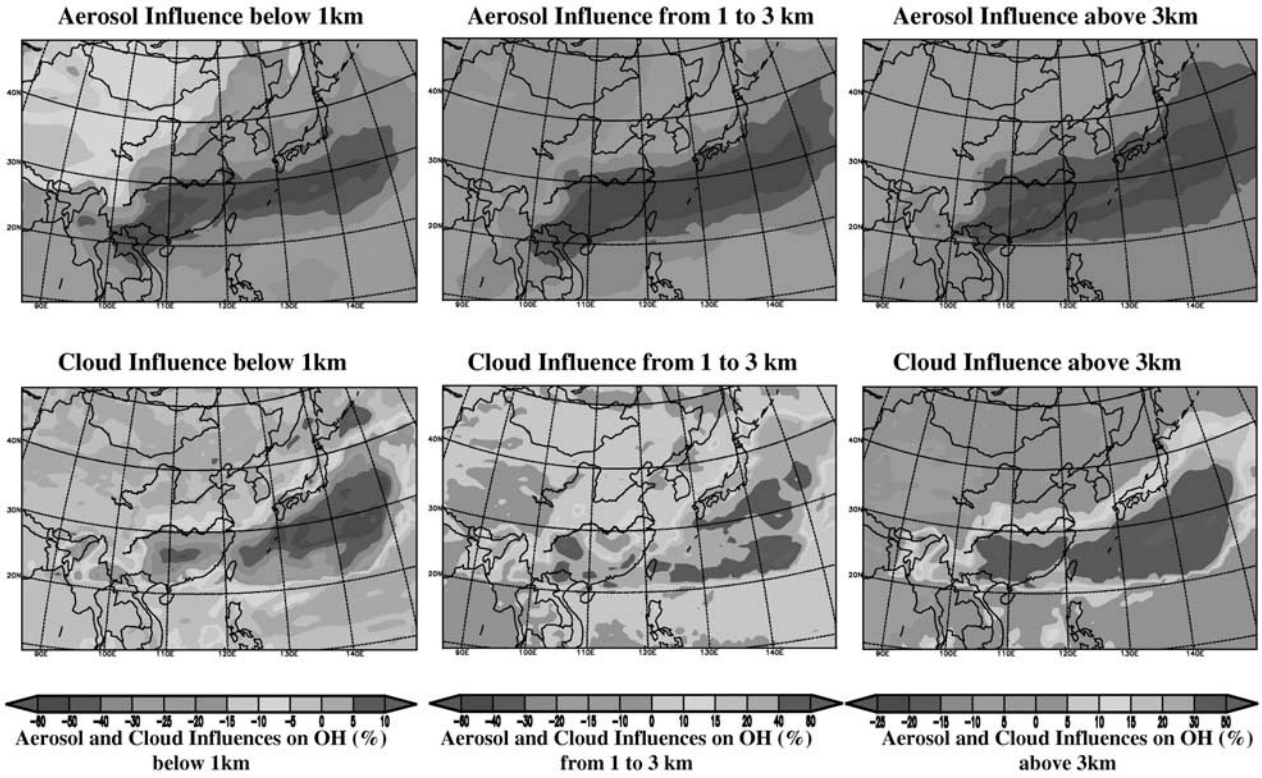

Figure 8. March-averaged aerosol and cloud influences on daytime OH in three layers: below 1 km, 1 to 3 km and above 3 km, represented in percentage change. See color version of this figure at back of this issue.

NO_x, which has very low background concentrations, and are more sensitive to the change of photochemical status than O_3. Figure 10 shows this. The daytime NO_x concentrations increased up to 40% in Shanghai plumes due to aerosol influences below 1km. Our simulation shows that the BB aerosol leads to a broad region extending from Southeast Asia to East China sea where the NO_x enhancement is generally more than 20% below 1 km for March. The cloud influence on NO_x is similar to that of aerosol at low altitudes, though their regions of influence are different. The cloud shielding effect can also cause the enhancement of NO_x by up to 40% in relatively clear sites, where the absolute NO_x concentrations are relatively low. Aerosols and clouds reduce the photolysis rates and lead to the enhancement of NO_x and also cause the corresponding decrease of NO_z concentrations. Over the east and south coasts of China, in the areas affected by the city plumes, including Beijing, Guangzhou, Hong Kong, and Shanghai, the averaged daytime PAN concentrations decreased by more than 10% due to aerosol influence below 1 km. The averaged PAN reduction caused by clouds was more than 5% in South China, where the cloud activity is strong during this period.

5. A Case Study on 27 March

[32] In the previous sections we have focused on mission-wide perspectives. Analysis of specific flights provides excellent opportunities to rigorously test our ability to model photolysis rates and to explore in detail the impacts of clouds and aerosols. Here we present a case study of the flights on 27 March. From 26–27 March, satellite images show that a continuous cloud band extended from the South China Sea to east of China, and then to the south of Japan. Fractional clouds covered Central China, North Korean, and the Japan Sea. During this period, a cold front moved southeastward over the East China Sea and the western Pacific. A weak low-pressure center existed east of Japan on 26 March and disappeared on 27 March. The cloud belt moved along with this front. Both the DC-8 and P-3 flew missions on 27 March; the P-3 encountered a volcanic plume, and the DC-8 explored frontal activities. Figure 11 shows these two flight paths mapped onto the GMS-5 satellite image (infrared color enhanced). Both of the aircrafts started and ended their flights in Yokota, near Tokyo.

[33] On 27 March, the 17th P-3 flight flew over a small area of the western Pacific, east of Japan. The main purpose of this flight was to observe the volcanic plumes emitted from Mt. Miyakejima. The P-3 flight-log recorded some visible cumulus clouds but no persistent overcast clouds. During the same day, the DC-8 aircraft operated over a much bigger area with overcast clouds at multiple layers. Along the 15th DC-8 flight path shown in Figure 11, the DC-8 flew west along latitude 23.5°N. In the second boundary layer run, overcast clouds at multiple layers, fog, and rain were recorded. Then the DC-8 headed north

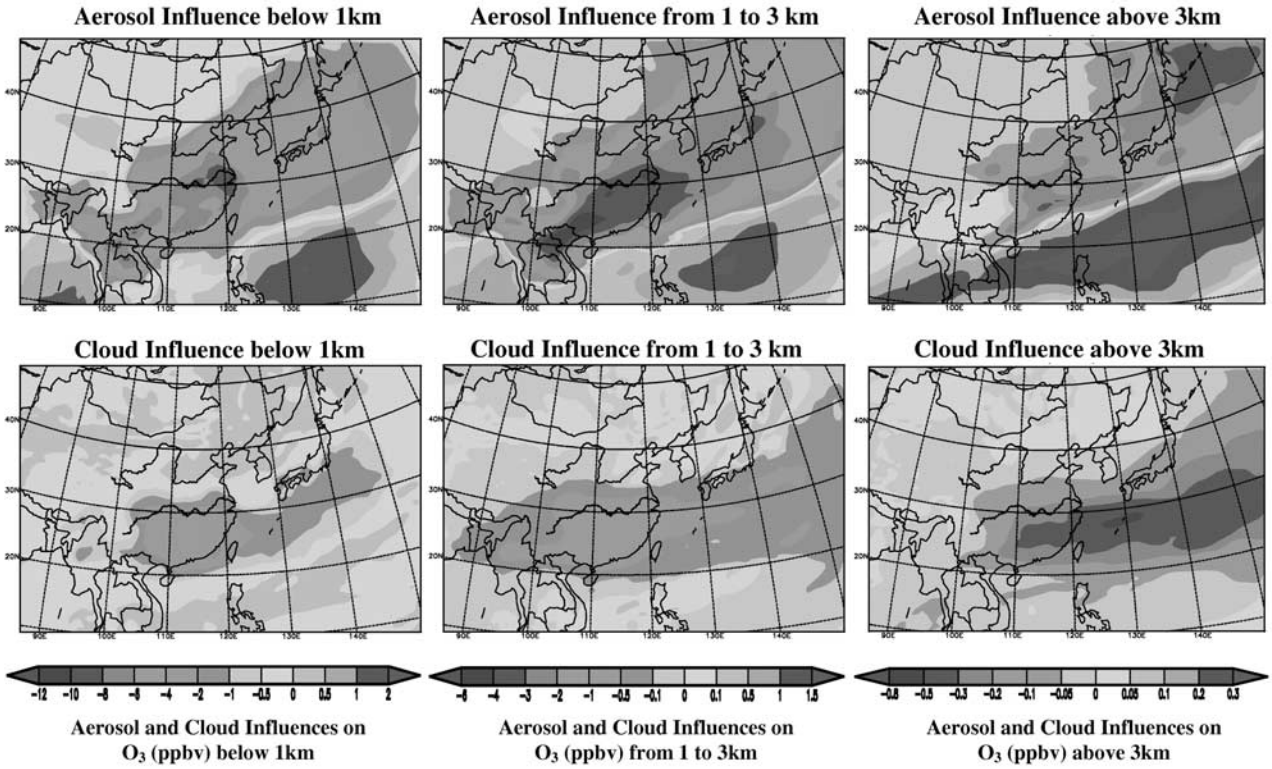

Figure 9. March-averaged aerosol and cloud influences on daytime ozone in three layers: below 1 km, 1 to 3 km and above 3 km. See color version of this figure at back of this issue.

to the Yellow Sea and found broken overcast clouds at multiple levels. On its way back to Japan the DC-8 aircraft performed two final boundary layer runs. Overcast stratocumulus with cloud bases near 1.6 km and an overcast deck of altostratus near 6 km were found. Clouds were very active during the DC-8 flight 15.

[34] Figure 12 shows the comparison of observed and simulated J[NO_2] for the three model cases along the DC-8 flight 15 and P-3 flight 17 paths. This figure also shows simulated and observed aerosol extinction coefficients for the P-3 flight and relative humidity (RH) for the DC-8 flight. Observed J-values on the DC-8 clearly show enhancements of photolysis rates above clouds and decreases of rates below clouds. Cloud positions can be estimated by the peak RH (>90%) in the altitude from 500 m to 3 km (Figure 12). Our meteorological prediction yielded

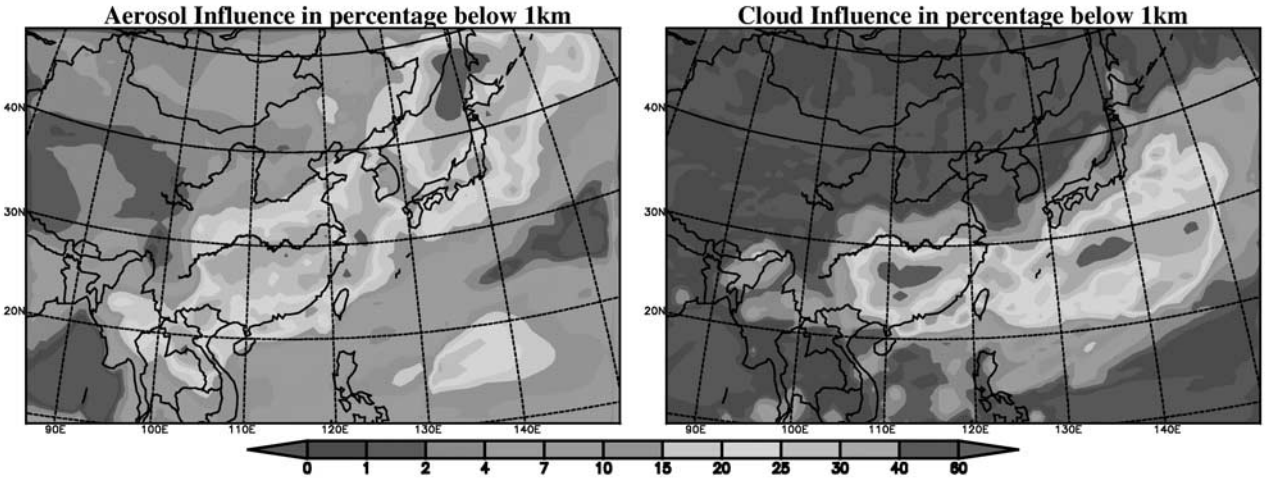

Figure 10. March-averaged aerosol and cloud influences on daytime NO_x below 1 km, represented in percentage change (%). See color version of this figure at back of this issue.

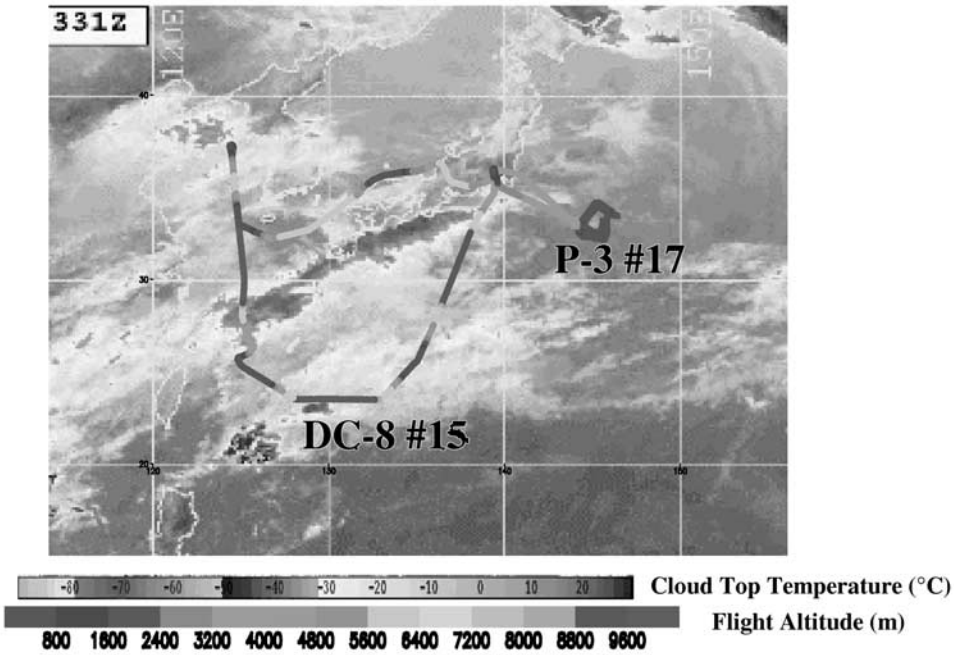

Figure 11. The flight paths of the 15th DC-8 flight and 17th P-3 flight on 27 March 2001, mapped on GMS-5 image (enhanced infrared color). See color version of this figure at back of this issue.

reasonable RH values. The NORMAL simulation successfully described the cloud influences along the DC-8 flight path, though it overestimated the cloud-shielding impact at lower altitudes. The CLEARSKY case systematically overestimated J-values below clouds and underestimated J-values above clouds. The CLEARSKY simulated J[NO_2] show a much weaker variation with altitude than observed. The NOAOD simulation slightly overestimated J[NO_2] at

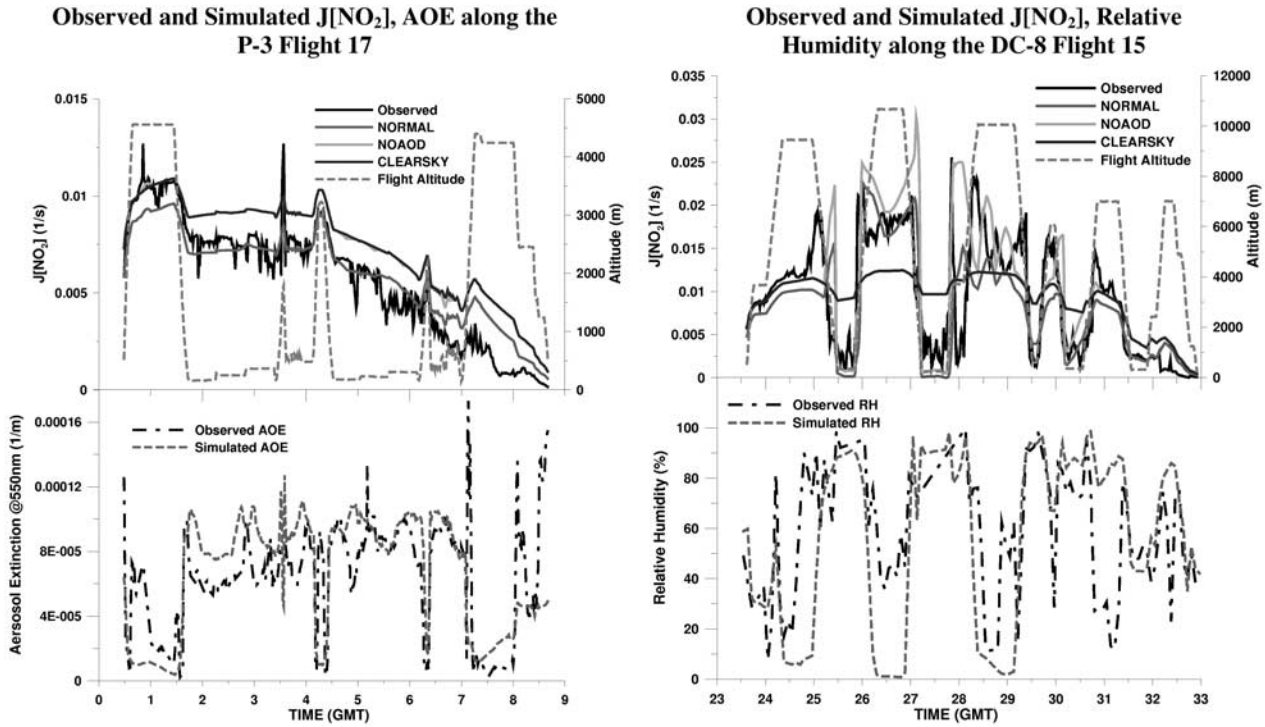

Figure 12. Observed and simulated J[NO_2] under the three conditions and associated physical parameters along with the flight paths of P-3 flight 17 and DC-8 flight 15. See color version of this figure at back of this issue.

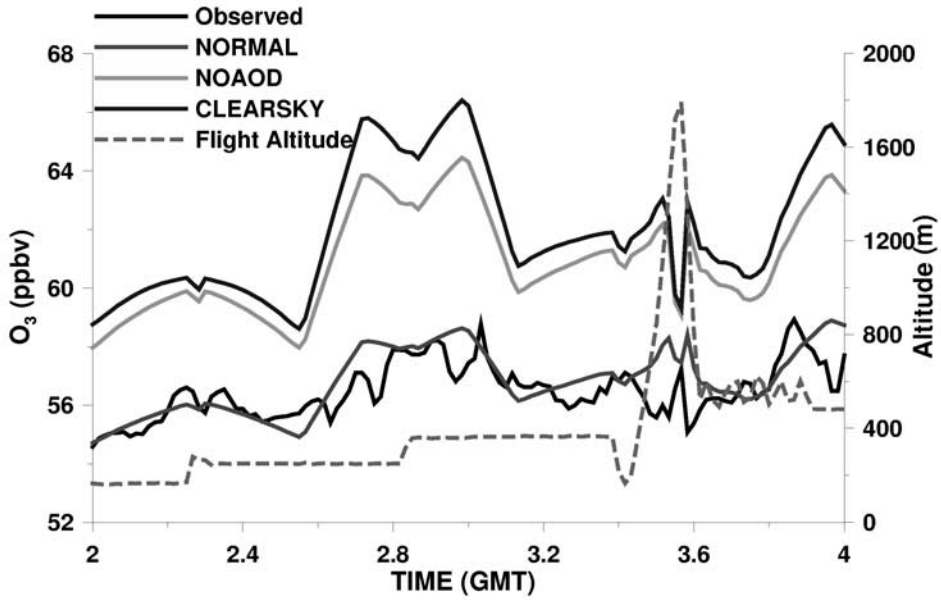

Figure 13. Observed and simulated ozone concentrations under the three conditions along with the flight paths of P-3 flight 17 from 2 to 4 GMT. See color version of this figure at back of this issue.

altitudes above 5 km. Generally the aerosol influence on J-values during the DC-8 flight 15 is much weaker than the cloud influence. In contrast the aerosol influence dominated on the P-3 flight 17. Since this P-3 flight encountered few clouds, the simulated J[NO_2] by NOAOD and CLEARSKY are nearly the same. Calculations without aerosols overestimated J[NO_2], and the NORMAL case best described the observed values. Figure 12 shows the simulated AOE agrees well with the observation.

[35] Figure 13 shows the observed and simulated O_3 level for the various cases during the period from 2 to 4 GMT (roughly 1100 to 1300 local time). During this period, the NORMAL case accurately represented the observed ozone levels, while the NOAOD case overestimated O_3 by up to 8 ppbv, and the CLEARSKY case overestimated ozone by up to 10 ppbv. To better understand the reasons for these differences, 5-day back trajectories along the P-3 flight path were calculated and are shown in Figure 14. The back trajectories show that airmasses observed on the P-3 during this time period passed by Tokyo and nearby areas at low altitudes. Before passing by Tokyo, some airmasses were transported off the east China coast, and over the Korean megacities of Seoul and Pusan. The ozone production along one trajectory is also shown. Along this trajectory we see the influence of aerosols. When we ignore the aerosol influence, ozone production is increased about 10 ppbv/hour in the Shanghai plume. Increased ozone production for the case NOAOD continues along the trajectory as fresh emissions are injected into this air mass. During nighttime periods, the O_3 difference between these two simulations did not increase because photochemical reactions were shutdown, and mixing with background airmass tends to reduce the differences. The effects of aerosols on O_3 levels are estimated to be about 8 ppbv for the segment that the P-3 aircraft encountered.

[36] These results clearly show that aerosol influences on chemical species depend on the airmass history and integration along the transport path. Thus these impacts cannot be assessed solely by local measurements.

6. Conclusions

[37] In this paper, we successfully utilized the three-dimensional STEM model with detailed photochemistry and explicit photolysis calculations to simulate the TRACE-P airborne observations. The model is shown to have substantial skill in calculating photolysis rates over a broad range of cloud and aerosol conditions. Sensitivity studies were performed to further identify how aerosol and clouds influence photolysis rates and subsequent trace gas distributions. These studies showed that both clouds and aerosols can impose significant impacts on J-values, short-lifetime radicals, and long-lived photochemical products and precursor species and that the intensities of these impacts vary from scenario to scenario. In general the presence of clouds reduces photolysis rates below cloud and increases the rates above clouds. Asian aerosols are shown to largely reduce photolysis rates throughout the column. Short-lived photochemical species, like OH, HO_2, and RO_2, respond in accordance to local changes in J-values and to local values of water vapor, methane, CO, and other primary species. However, the influence of aerosols and clouds through photolysis rates on longer-lived species and secondary photochemical products is shown to be nonlocal and instead dependent on the integrated history of the air mass. This is particularly important for the aerosol influence, as aerosols and precursor species are typically emitted and transported together in Asia, providing a longer period for aerosols to exert their influence.

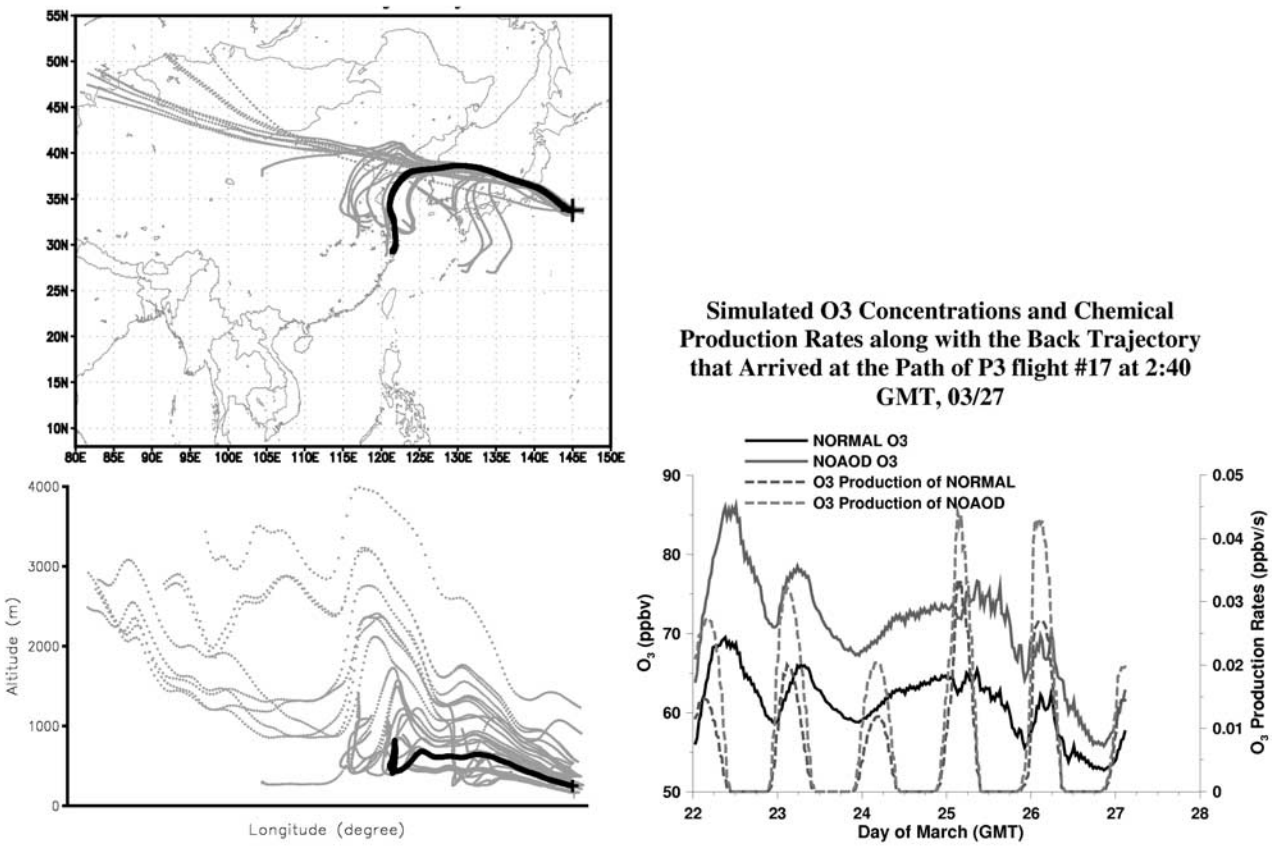

Figure 14. The back trajectories that reached the paths of P-3 flight 17 from 2 to 4 GMT, 27 March. The bold black line at the left plot refers to the trajectory path along with which we extract the O_3 concentrations and production rates, shown in the right plot. See color version of this figure at back of this issue.

[38] For these reasons we found that during the TRACE-P period, the three-dimensional influence of aerosols on primary chemical species are on average stronger than cloud influences. Aerosols are shown to decrease J-values, slow down the photochemical reactions, increase concentrations of NO_x and NMHCs, and reduce the photochemical products like NO_z (NO_y-NO_x) and O_3. These influences on photochemical processes are particularly significant in biomass burning and megacity plumes because these plumes contain abundant pollutants and aerosols. The Asia-Pacific region is an aerosol-rich area: China has the highest coal consumption in the world, dust storms appear frequently during springtime, seasonal biomass burning contributes large amounts of BC and OC, biofuel is widely used in the countryside, and large volcanoes exist in the western Pacific. Our case study for P3 flight 17 presented a clear example of how the aerosol influences occur along the air mass transport path.

[39] This study showed that aerosol and cloud influences are very important to the photochemical processes. The aerosol influence on radiation is to reduce J-values and extend the lifetime of NO_x, NMHCs, and CO, which increases the export of pollutants off the continent. For example, March-averaged NO_x concentrations in the lowest layers of the troposphere were enhanced 40% due to aerosol influences in the Shanghai plume region.

[40] This study clearly shows the importance of accounting for the aerosol influence on photolysis rates in this region and suggests the consideration of this influence in global, regional, and local air quality and atmospheric chemistry studies. An accurate treatment of these interactions requires detailed information of clouds and aerosol size, composition, and optical properties. Furthermore, since these impacts are nonlocal, a better understanding of the air mass history is required. These issues place increased demand on models and measurement strategies. Finally, it is important to note that in this paper we only studied the effect of aerosols via changing photolysis rates. The direct surface reactions on aerosols can either exacerbate or modulate the effects presented here.

[41] **Acknowledgments.** This work was supported by NASA GTE TRACE-P, ACMAP, and the NSF Atmospheric Chemistry program. We appreciate Sacha Madronich providing the TUV model under GNU General Public License.

References

Carmichael, G. R., et al., Regional-scale chemical transport modeling in support of intensive field experiments: Overview and analysis of the TRACE-P observations, *J. Geophys. Res.*, *108*(D21), 8823, doi:10.1029/2002JD003117, in press, 2003.

Carter, W., Documentation of the SAPRC-99 chemical mechanism for voc reactivity assessment, *Final Report to California Air Resources Board, Contract 92-329*, Univ. of Calif., Riverside, Riverside, Calif., 2000.

Damian, V., A. Sandu, M. Damian, F. Potra, and G. R. Carmichael, The kinetic preprocessor KPP a software environment for solving chemical kinetics, *Comput. Chem. Eng.*, *26*, 1567–1579, 2002.

Dickerson, R. R., S. Kondragunta, G. Stenchikov, K. L. Civerolo, B. G. Doddridge, and B. N. Holben, The impact of aerosols on solar ultraviolet radiation and photochemical smog, *Science*, *278*, 827–830, 1997.

Ebert, E. E., and J. A. Curry, A parameterization of ice-cloud optical-properties for climate models, *J. Geophys. Res.*, *97*, 3831–3836, 1992.

Guenther, A., et al., A global-model of natural volatile organic-compound emissions, *J. Geophys. Res.*, *100*, 8873–8892, 1995.

Jacob, D. J., J. H. Crawford, M. M. Kleb, V. E. Conners, R. J. Bendura, J. L. Raper Jr., G. W. Sachse, J. C. Gille, and L. Emmons, The Transport and Chemical Evolution over the Pacific (TRACE-P) mission: Design, execution, and overview of results, *J. Geophys. Res.*, *108*(D20), 8781, doi:10.1029/2002JD003276, in press, 2003.

Jordan, C. E., et al., Chemical and physical properties of bulk aerosols within four sectors observed during TRACE-P, *J. Geophys. Res.*, *108*(D21), 8817, doi:10.1029/2002JD003101, in press, 2003.

Lefer, B., R. Shetter, S. Hall, J. Crawford, J. Olson, G. R. Carmichael, and Y. Tang, Impact of clouds and aerosols on photolysis frequencies and photochemistry during TRACE-P: 1. Analysis using radiative transfer and photochemical box models, *J. Geophys. Res.*, *108*(D21), 8821, doi:10.1029/2002JD003171, in press, 2003.

Liao, H., Y. L. Yung, and J. H. Seinfeld, Effects of aerosols on tropospheric photolysis rates in clear and cloudy atmospheres, *J. Geophys. Res.*, *104*, 23,697–23,707, 1999.

Liu, M., and D. L. Westphal, A study of the sensitivity of simulated mineral dust production to model resolution, *J. Geophys. Res.*, *106*, 18,099–18,112, 2001.

He, S., and G. R. Carmichael, Sensitivity of photolysis rates and ozone production in the troposphere to aerosol properties, *J. Geophys. Res.*, *104*, 26,307–26,324, 2001.

Hess, M., P. Koepke, and I. Schult, Optical properties of aerosols and clouds: The software package OPAC, *Bull. Am. Meteorol. Soc.*, *79*(5), 831–844, 1998.

Madronich, S., Photodissociation in the atmosphere: 1. Actinic flux and the effects of ground reflections and clouds, *J. Geophys. Res.*, *92*, 9740–9752, 1987.

Madronich, S., and S. Flocke, The role of solar radiation in atmospheric chemistry, in *Handbook of Environmental Chemistry*, edited by P. Boule, pp. 1–26, Springer-Verlag, New York, 1999.

Martin, R. V., D. J. Jacob, R. M. Yantosca, M. Chin, and P. Ginoux, Global and regional decreases in tropospheric oxidants from photochemical effects of aerosols, *J. Geophys. Res.*, *108*, doi:10.1029/2003JD003806, in press, 2003.

Martin, T. J., B. G. Gardiner, and G. Seckmeyer, Uncertainties in satellite-derived estimates of surface UV doses, *J. Geophys. Res.*, *105*, 27,005–27,011, 2000.

McRae, G. J., W. R. Goodin, and J. H. Seinfeld, Numerical solution of the atmospheric diffusion equation for chemical reacting flows, *J. Comput. Phys.*, *45*, 1–42, 1982.

Miehe, P., A. Sandu, G. R. Carmichael, Y. Tang, and D. Daescu, A communication library for the parallelization of air quality models on structured grids, *Atmos. Environ.*, *36*, 3917–3930, 2002.

Monahan, E. C., D. E. Spiel, and K. L. Davidson, A model of marine aerosol generation via whitecaps and wave disruption, in *Oceanic Whitecaps*, edited by E. C. Monahan and G. MacNiocaill, pp. 167–174, D. Reidel, Norwell, Mass., 1986.

Nickling, W. G., and J. A. Gillies, Dust emission and transport in Mali, West Africa, *Sedimentology*, *40*, 859–868, 1993.

Olivier, J. G. J., A. F. Bouwman, C. W. M. Van der Maas, J. J. M. Berdowski, J. P. J. Bloos, A. J. H. Visschedijk, P. Y. J. Zandveld, and J. L. Haverlag, Description of EDGAR Version 2.0: A set of global emission inventories of greenhouse gases and ozone-depleting substances for all anthropogenic and most natural sources on a per country basis and on 1° × 1° grid, *RIVM/TNO report 771060002*, Natl. Inst. of Public Health and the Environ., Bilthoven, Netherlands, 1996.

Pickering, K. E., Y. S. Wang, W. K. Tao, C. Price, and J. F. Muller, Vertical distributions of lightning NOx for use in regional and global chemical transport models, *J. Geophys. Res.*, *103*, 31,203–31,216, 1998.

Shetter, R. E., L. Cinquini, B. L. Lefer, S. R. Hall, and S. Madronich, Comparison of airborne measured and calculated spectral actinic flux and derived photolysis frequencies during the PEM Tropics B mission, *J. Geophys. Res.*, *108*(D2), 8234, doi:10.1029/2001JD001320, 2002.

Streets, D. G., et al., An inventory of gaseous and primary aerosol emissions in Asia in the year 2000, *J. Geophys. Res.*, *108*(D21), 8809, doi:10.1029/2002JD003093, in press, 2003.

Tang, Y., et al., Influences of biomass burning during TRACE-P experiment identified by the regional chemical transport model, *J. Geophys. Res.*, *108*(D21), 8824, doi:10.1029/2002JD003110, in press, 2003a.

Tang, Y., et al., Dust outflows and their impacts on regional chemistry during ACE-ASIA experiment: A model study, *J. Geophys. Res.*, *108*, doi:10.1029/2002JD003806, in press, 2003b.

Tremback, C. J., Numerical simulation of a mesoscale convective complex: Model development and numerical results, Ph.D. dissertation, Atmos Sci. paper 465, Department of Atmos. Sci., Colorado State Univ., Fort Collins, Colo., 1990.

Verwer, J. G., E. J. Spee, J. G. Blom, and W. H. Hundsdorfer, A second order Rosenbrock method applied to photochemical dispersion problems, *SIAM J. Sci. Comput.*, *20*(4), 1456–1480, 1999.

Walko, R. L., W. R. Cotton, M. P. Meyers, and J. Y. Harrington, New RAMS cloud microphysics parameterization, part I: The single-moment scheme, *Atmos. Res.*, *28*, 29–62, 1995.

Weber, R. J., et al., New particle formation in anthropogenic plumes advecting from Asia observed during TRACE-P, *J. Geophys. Res.*, *108*(D21), 8814, doi:10.1029/2002JD003112, in press, 2003.

Wesely, M. L., Parameterization of surface resistances to gaseous dry deposition in regional-scale numerical models, *Atmos. Environ.*, *23*, 1293–1304, 1989.

Woo, J. H., et al., Contribution of biomass and biofuel emissions to trace gas distributions in Asia during the TRACE-P experiment, *J. Geophys. Res.*, *108*(D21), 8812, doi:10.1029/2002JD003200, in press, 2003.

B. E. Anderson and M. A. Avery, Atmospheric Sciences Competency, NASA Langley Research Center, Hampton, VA 23681, USA. (b.e.anderson@larc.nasa.gov; m.a.avery@larc.nasa.gov)

D. R. Blake, Department of Chemistry, University of California, Irvine, Irvine, CA 92697, USA. (drblake@uci.edu)

G. R. Carmichael, H. Huang, Y. Tang, and J.-H. Woo, Center for Global and Regional Environmental Research, University of Iowa, Iowa City, IA 52242, USA. (gcarmich@engineering.uiowa.edu; huang@cgrer.uiowa.edu; ytang@cgrer.uiowa.edu; woojh21@cgrer.uiowa.edu)

A. D. Clarke, School of Ocean and Earth Science and Technology, University of Hawaii at Manoa, Honolulu, HI 96822, USA. (tclarke@soest.hawaii.edu)

G. Kurata, Department of Ecological Engineering, Toyohashi University of Technology, Toyohashi, Aichi 441-8580, Japan. (kurata@eco.tut.ac.jp)

B. Lefer and R. E. Shetter, National Center for Atmospheric Research, 1850 Table Mesa Dr., Boulder, CO 80305, USA. (lefer@ucar.edu; shetter@ucar.edu)

I. Uno, Research Institute for Applied Mechanics, Kyushu University, Fukuoka 816-8580, Japan. (iuno@riam.kyushu-u.acjp)

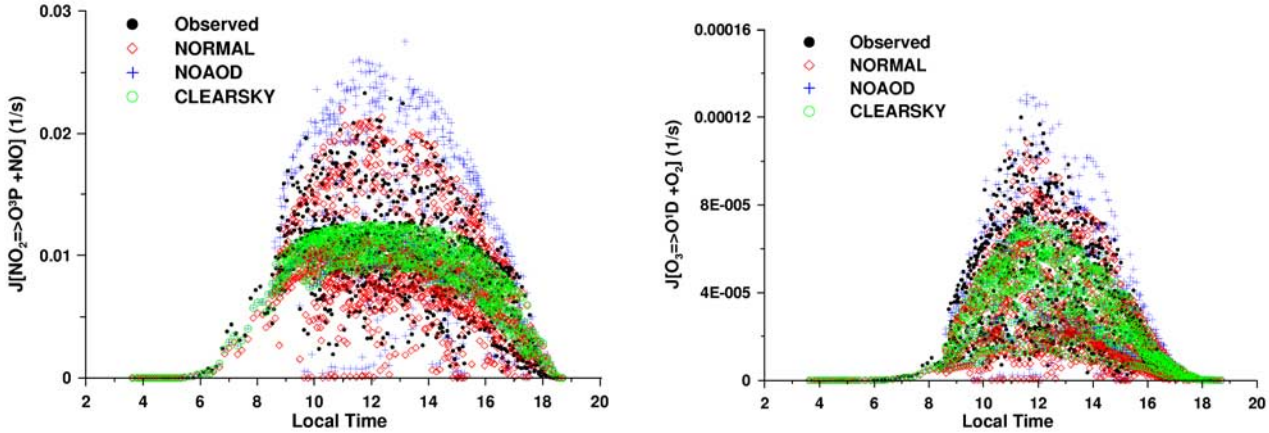

Figure 4. Observed and simulated J[NO_2], J[O^1D] for All TRACE-P DC-8 and P-3 flights under three conditions: NORMAL, NOAOD, and CLEARSKY, distributed in local time.

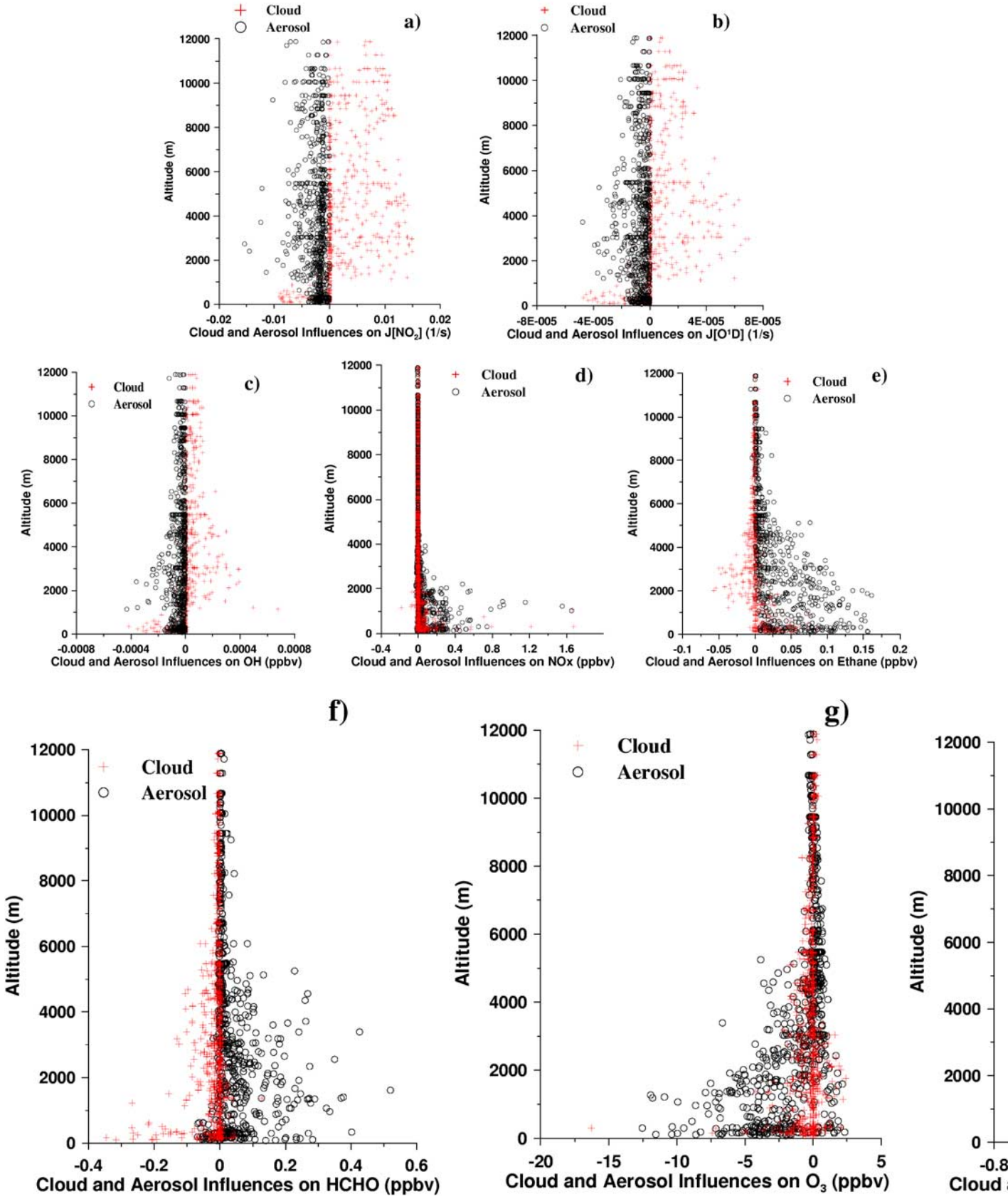

Figure 5. Observed and simulated aerosol and cloud influences on J[NO_2], J[O^1D], OH, NO_x, Ethane, HCHO, O_3, and PAN for all TRACE-P DC-8 and P3 flights in vertical profiles. The aerosol influences are represented in NORMAL minus NOAOD simulations, and clouds influences are represented in NOAOD minus CLEARSKY.

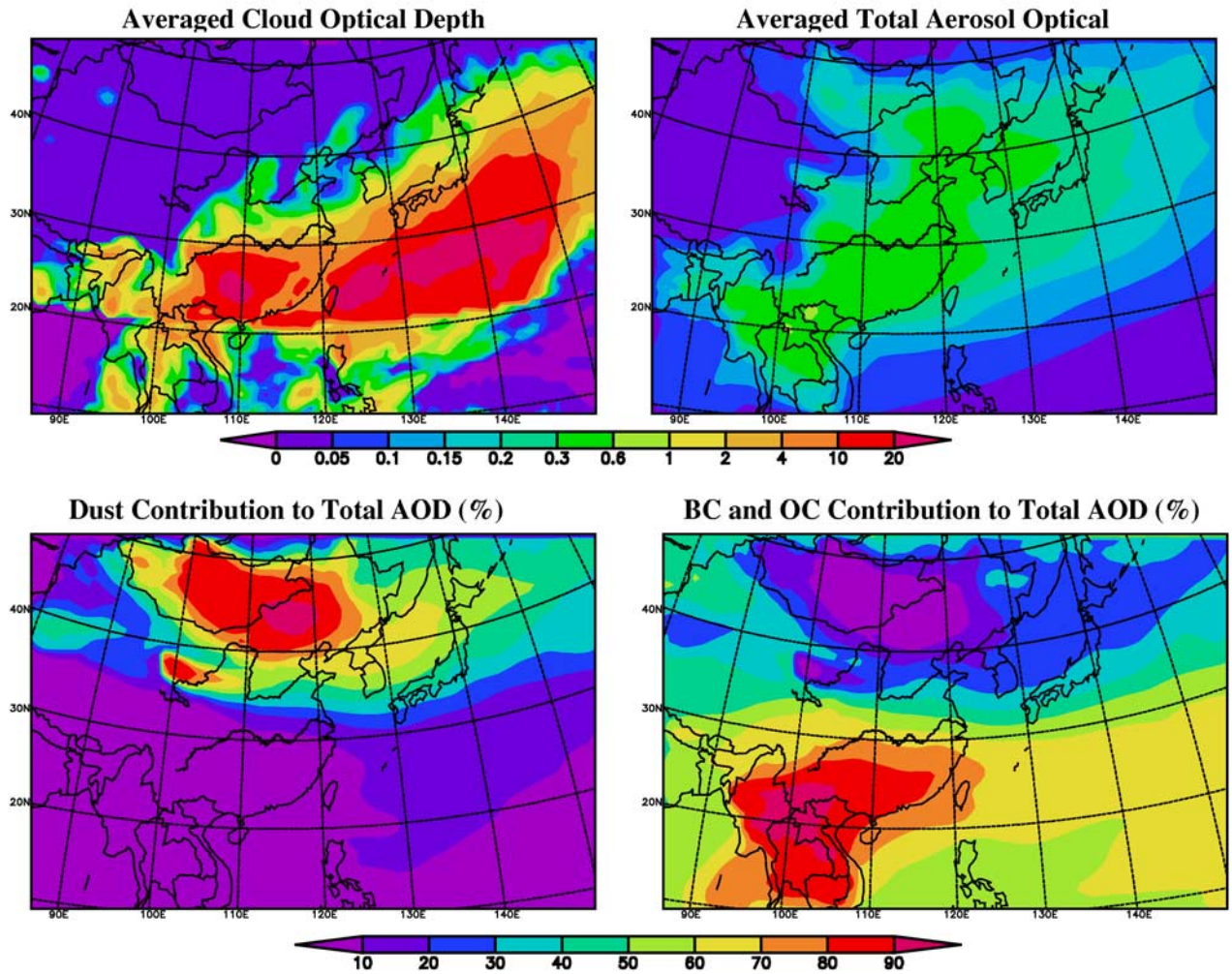

Figure 6. March-averaged simulated cloud optical depth, aerosols optical depth, and the fractional contributions from dust, BC, and OC.

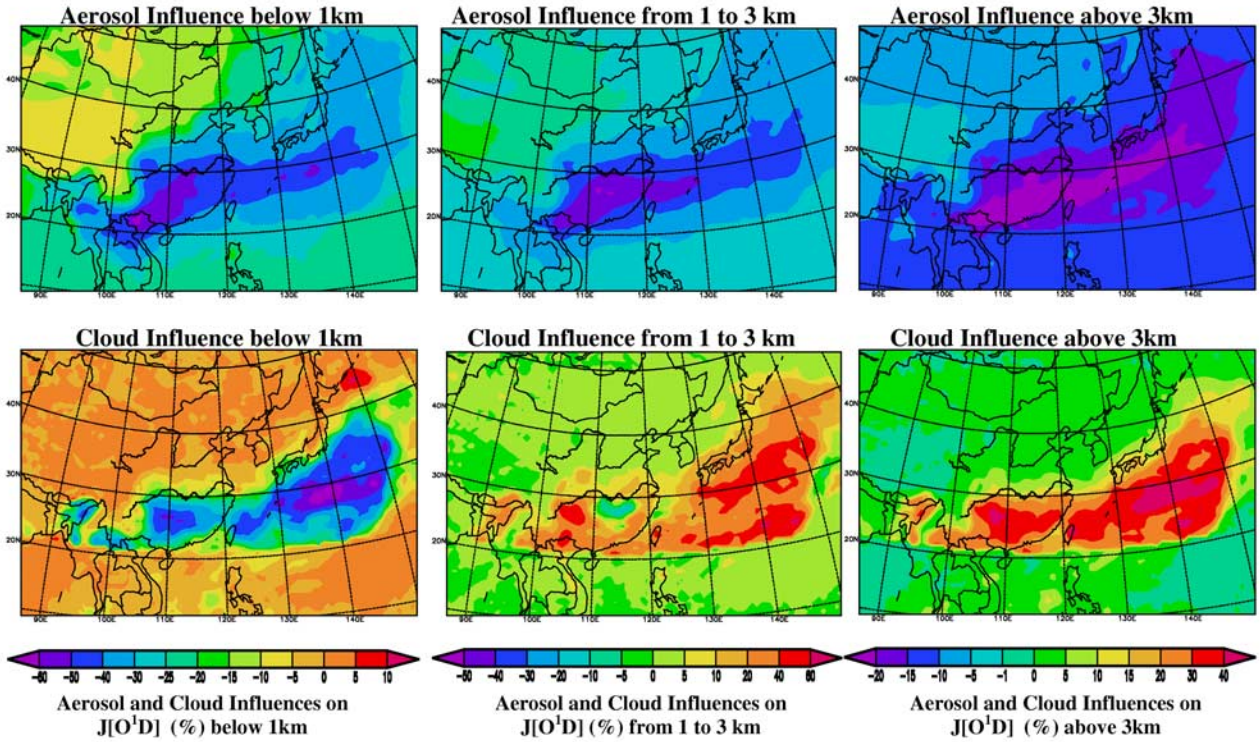

Figure 7. March-averaged aerosol and cloud influences on daytime J[O^1D] in three layers: below 1 km, 1 to 3 km, and above 3 km, represented in percentage change.

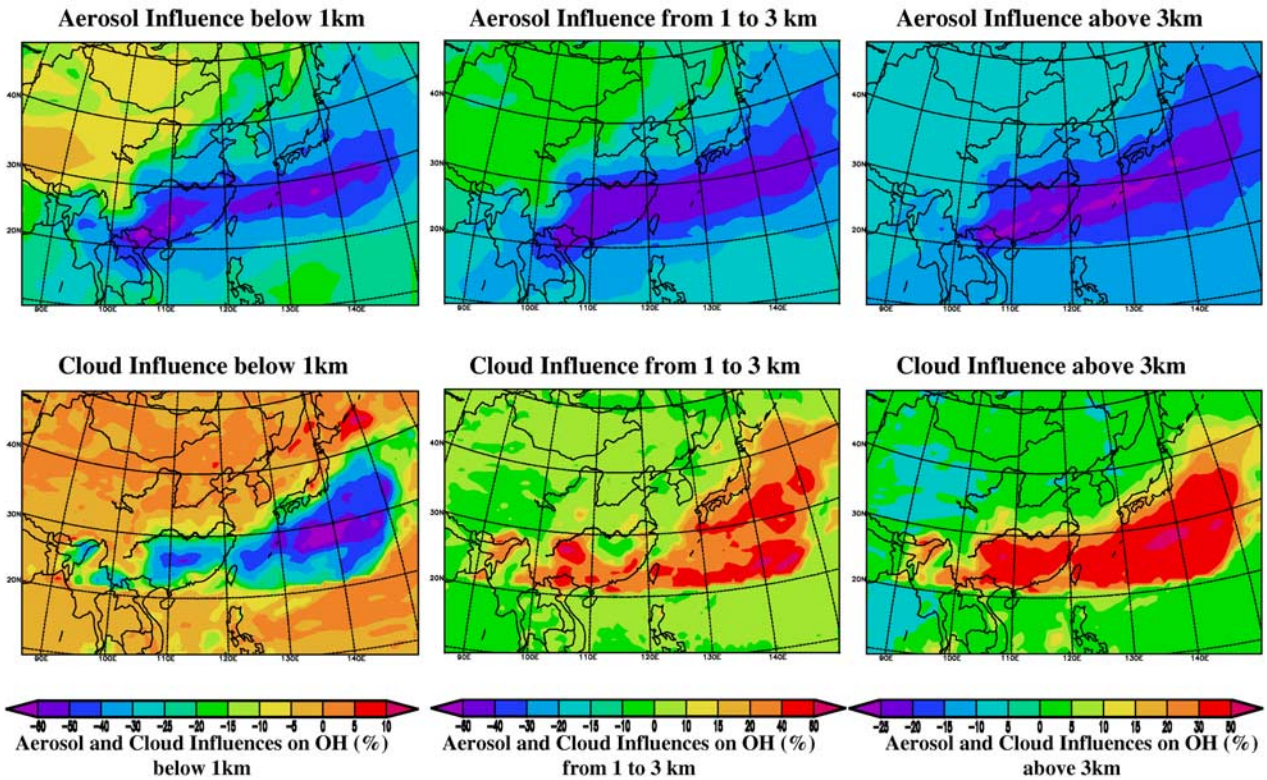

Figure 8. March-averaged aerosol and cloud influences on daytime OH in three layers: below 1 km, 1 to 3 km and above 3 km, represented in percentage change.

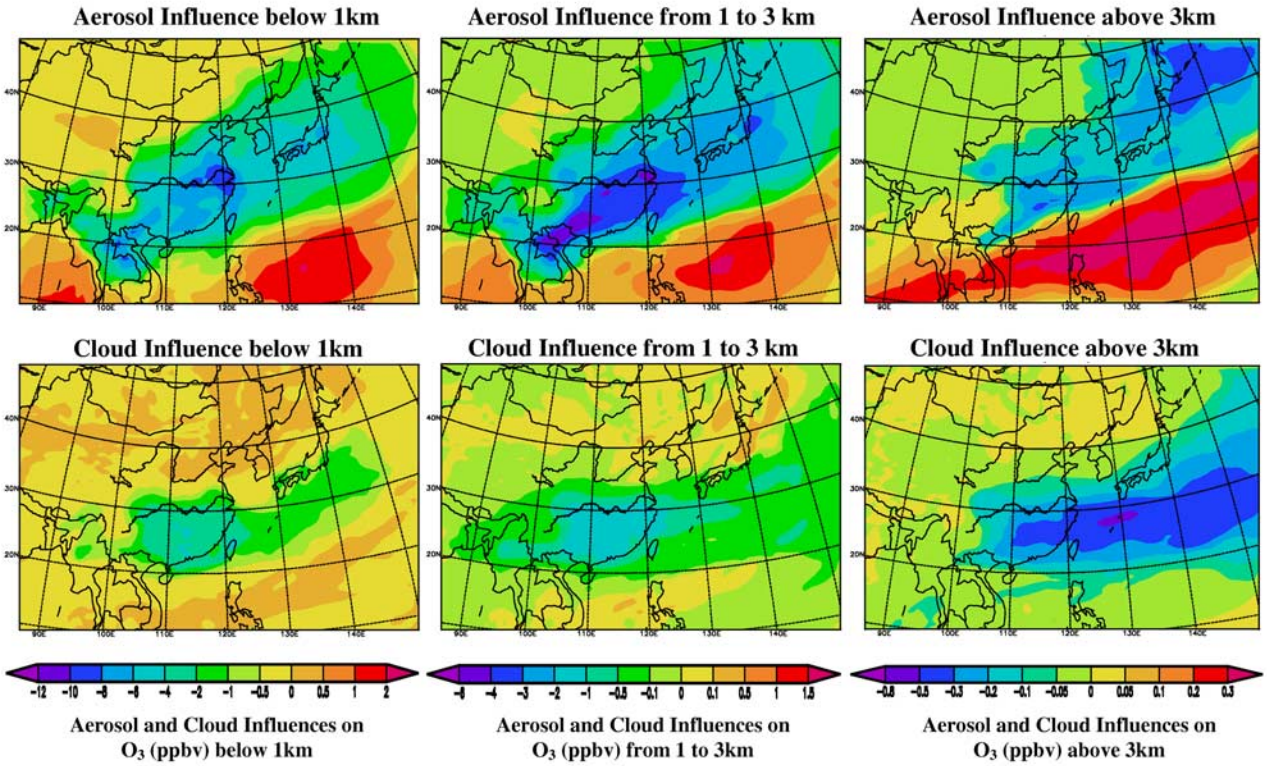

Figure 9. March-averaged aerosol and cloud influences on daytime ozone in three layers: below 1 km, 1 to 3 km and above 3 km.

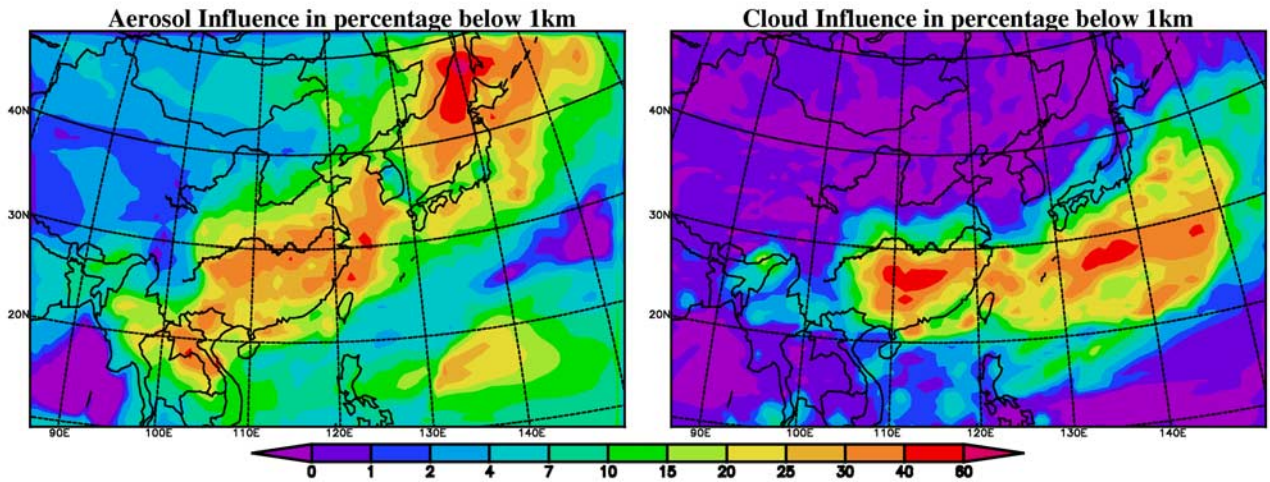

Figure 10. March-averaged aerosol and cloud influences on daytime NO_x below 1 km, represented in percentage change (%).

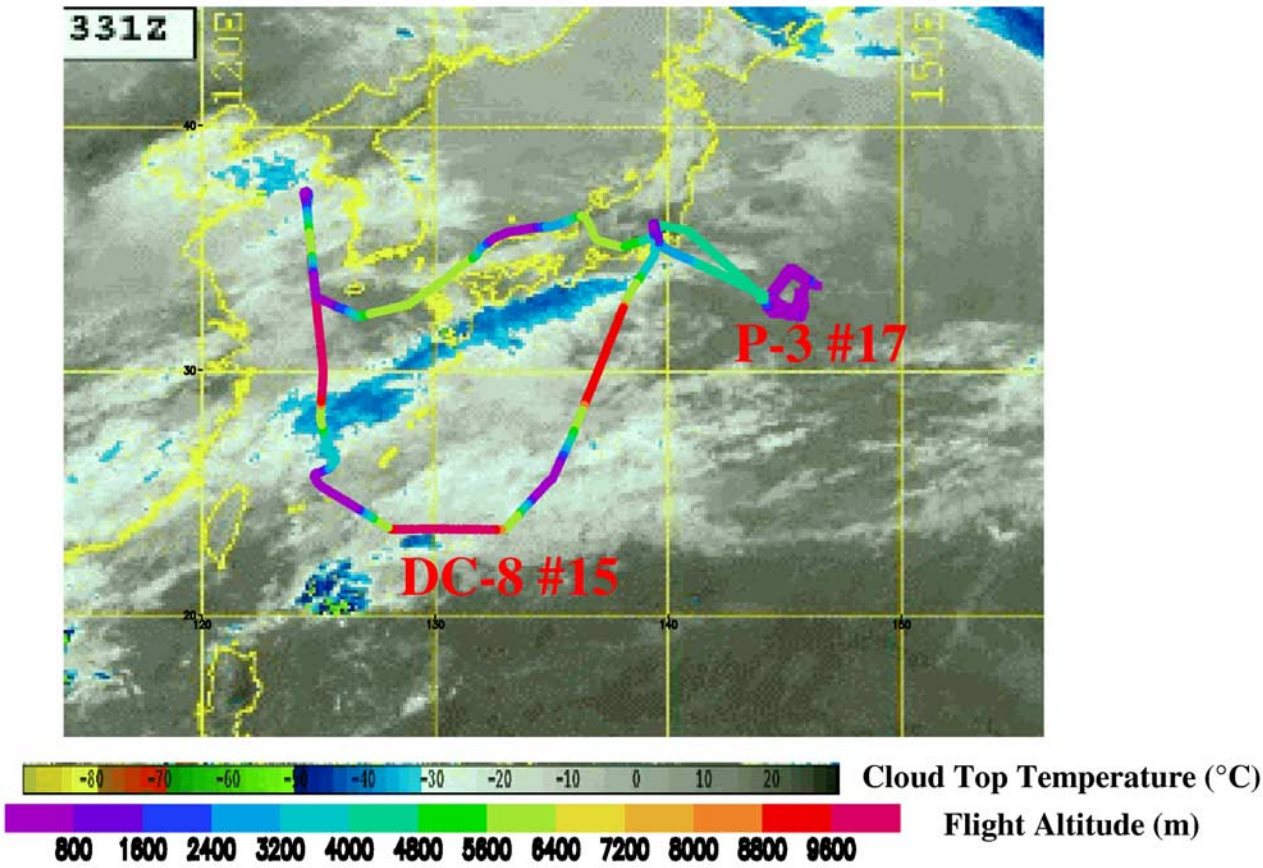

Figure 11. The flight paths of the 15th DC-8 flight and 17th P-3 flight on 27 March 2001, mapped on GMS-5 image (enhanced infrared color).

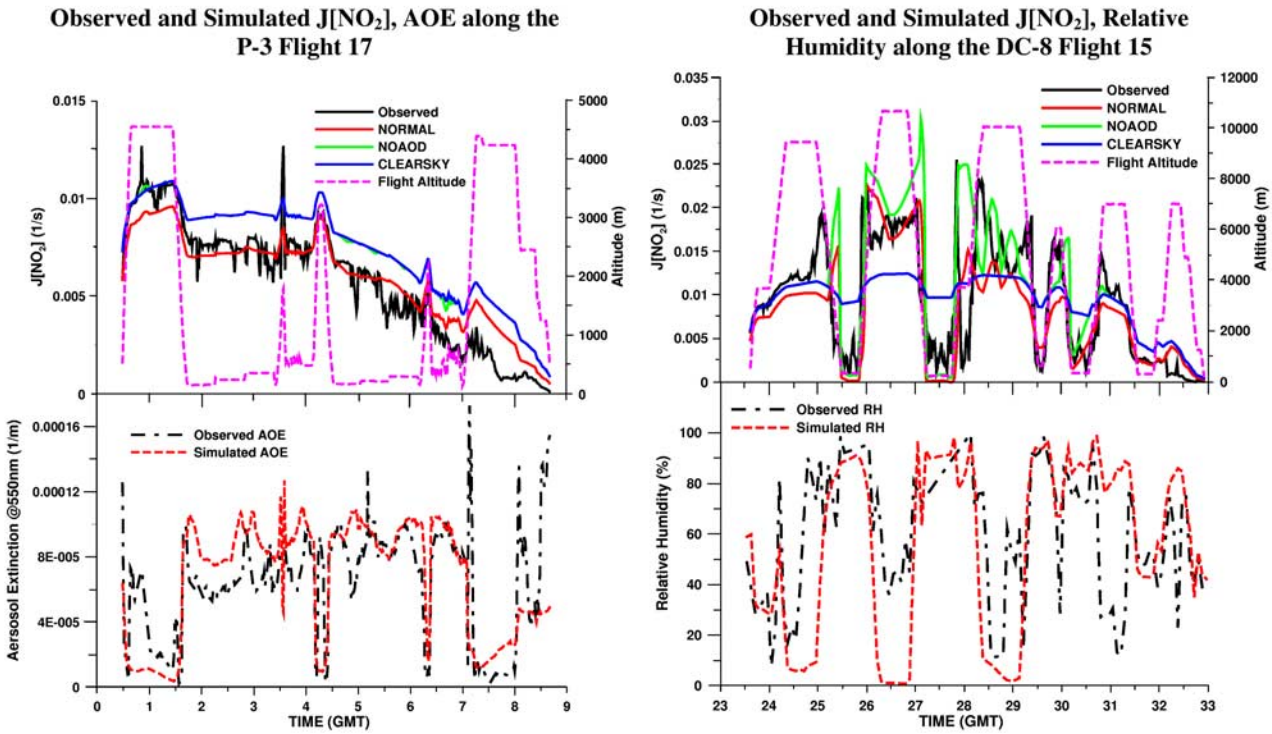

Figure 12. Observed and simulated $J[NO_2]$ under the three conditions and associated physical parameters along with the flight paths of P-3 flight 17 and DC-8 flight 15.

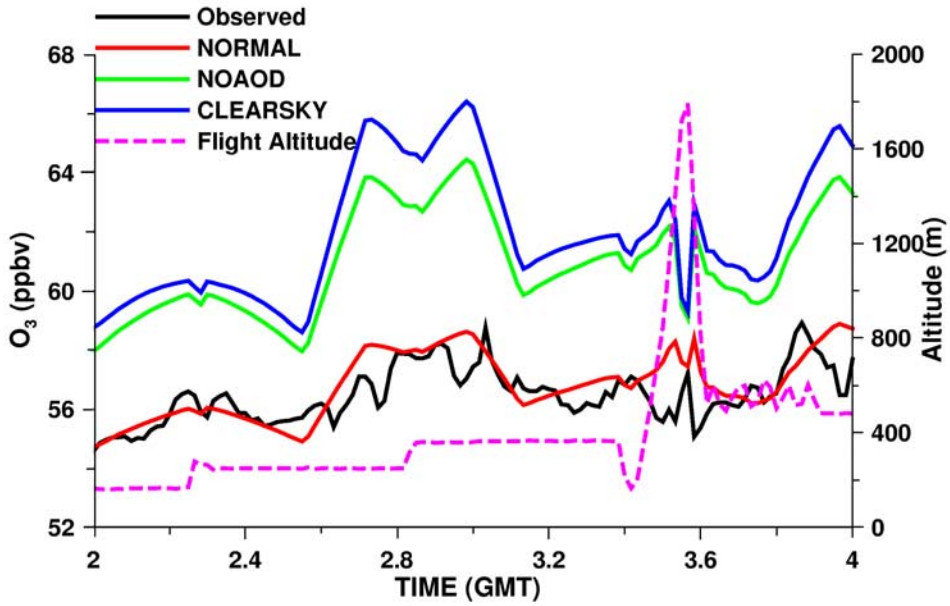

Figure 13. Observed and simulated ozone concentrations under the three conditions along with the flight paths of P-3 flight 17 from 2 to 4 GMT.

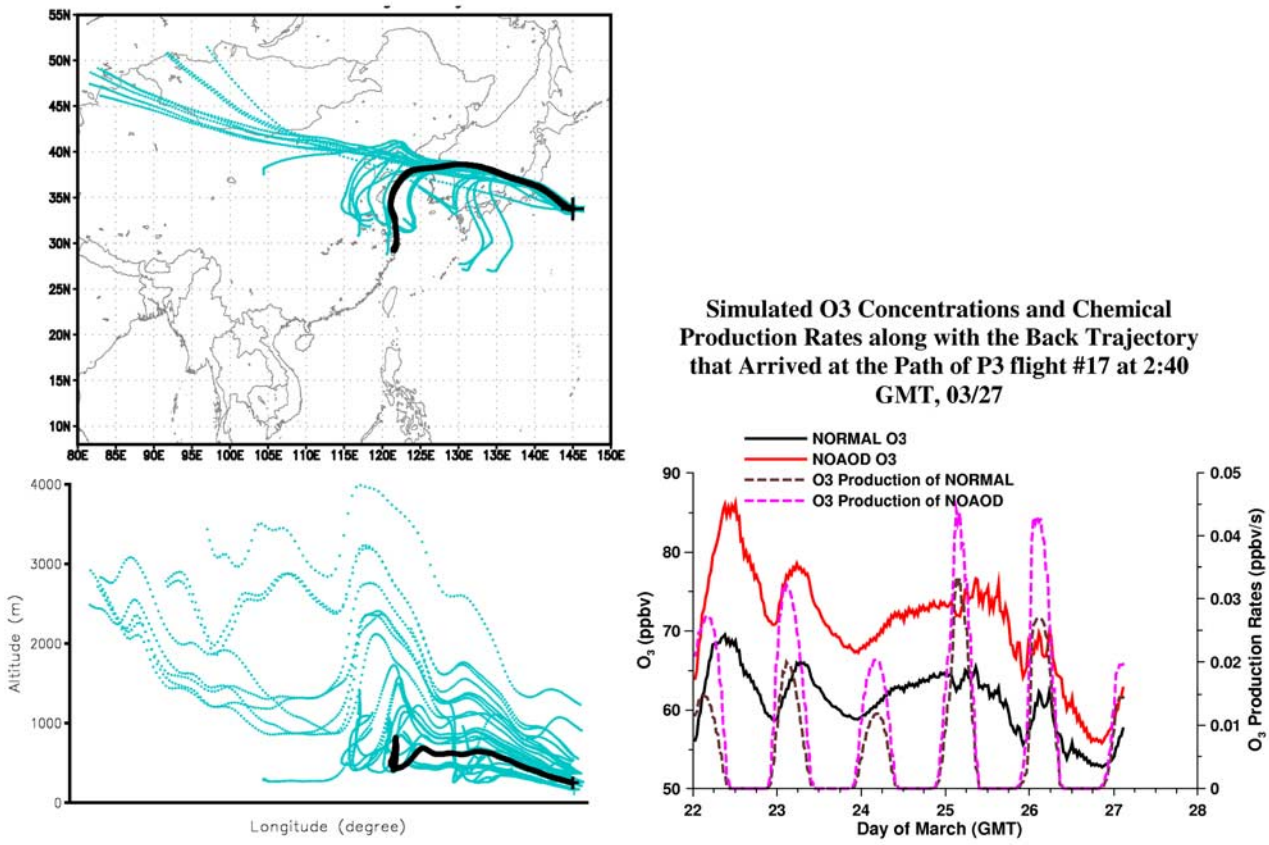

Figure 14. The back trajectories that reached the paths of P-3 flight 17 from 2 to 4 GMT, 27 March. The bold black line at the left plot refers to the trajectory path along with which we extract the O_3 concentrations and production rates, shown in the right plot.